



Scheme of negative acoustic radiation force based on a multiple-layered spherical structure

Menyang Gong(宫门阳), Xin Xu(徐鑫), Yupei Qiao(乔玉配), Jiehui Liu(刘杰惠), Aijun He(何爱军), and Xiaozhou Liu(刘晓宙)

Citation: Chin. Phys. B, 2024, 33 (1): 014302. DOI: 10.1088/1674-1056/acfa80

Journal homepage: <http://cpb.iphy.ac.cn>; <http://iopscience.iop.org/cpb>

What follows is a list of articles you may be interested in

Helical particle manipulation based on power-exponent-phase acoustic vortices generated by a sector transducer array

Qingdong Wang(王青东), Yantao Hu(胡彦涛), Shengli Wang(王胜利), and Hongyu Li(李洪宇)

Chin. Phys. B, 2023, 32 (6): 064304. DOI: 10.1088/1674-1056/acc800

Acoustic radiation force on a rigid cylinder near rigid corner boundaries exerted by a Gaussian beam field

Qin Chang(常钦), Yuchen Zang(臧雨宸), Weijun Lin(林伟军), Chang Su(苏畅), and Pengfei Wu(吴鹏飞)

Chin. Phys. B, 2022, 31 (4): 044302. DOI: 10.1088/1674-1056/ac2d1f

Axial acoustic radiation force on an elastic spherical shell near an impedance boundary for zero-order quasi-Bessel-Gauss beam

Yu-Chen Zang(臧雨宸), Wei-Jun Lin(林伟军), Chang Su(苏畅), and Peng-Fei Wu(吴鹏飞)

Chin. Phys. B, 2021, 30 (4): 044301. DOI: 10.1088/1674-1056/abca27

Radiation force and torque on a two-dimensional circular cross-section of a non-viscous eccentric layered compressible cylinder in acoustical standing waves

F G Mitri

Chin. Phys. B, 2021, 30 (2): 024302. DOI: 10.1088/1674-1056/abbbd9

Multiple off-axis acoustic vortices generated by dual coaxial vortex beams

Wen Li(李雯), Si-Jie Dai(戴思捷), Qing-Yu Ma(马青玉), Ge-Pu Guo(郭各朴), He-Ping Ding(丁鹤平)

Chin. Phys. B, 2018, 27 (2): 024301. DOI: 10.1088/1674-1056/27/2/024301

CPB

Chinese Physics B

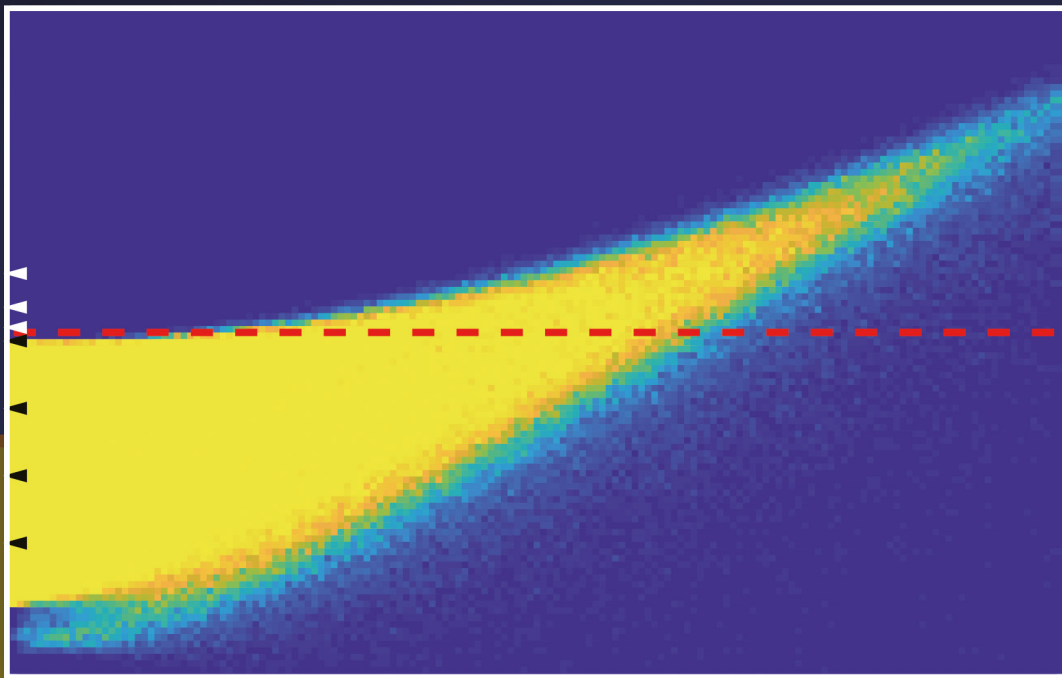
Volume 33 January 2024 Number 1

SPECIAL TOPIC

- Valleytronics
- States and new effects in nonequilibrium

A series Journal of the Chinese Physical Society Distributed by IOP Publishing

iopscience.org/cpb | cpb.iphy.ac.cn



Featured Article

Higher-order topological Anderson insulator on the Sierpiński lattice

Huan Chen, Zheng-Rong Liu, Rui Chen, Bin Zhou

Chin. Phys. B, 2024, 33: 017202

Chinese Physics B(中国物理B)

First published in 1992. Published monthly in hard copy by the Chinese Physical Society and online by IOP Publishing, No. 2 The Distillery, Glassfields, Avon Street, Bristol BS2 0GR, UK

Institutional subscription information: 2024 volume

For all countries, except the United States, Canada and Central and South America, the subscription rate per annual volume is UK £1629 (electronic only).

Orders to:

Journals Subscription Fulfilment, IOP Publishing, No. 2 The Distillery, Glassfields, Avon Street, Bristol BS2 0GR, UK

For the United States, Canada and Central and South America, the subscription rate per annual volume is US\$3245 (electronic only).

Orders to: IOP Publishing, P. O. Box 320, Congers, NY 10920-0320, USA

© 2024 Chinese Physical Society and IOP Publishing Ltd

All rights reserved. No part of this publication may be reproduced, stored in a retrieval system, or transmitted in any form or by any means, electronic, mechanical, photocopying, recording or otherwise, without the prior written permission of the copyright owner.

Editorial Office: Institute of Physics, Chinese Academy of Sciences, P. O. Box 603, Beijing 100190, China

Tel: (86-10) 82649026 or 82649519, Fax: (86-10) 82649027, E-mail: cpb@iphy.ac.cn

主管单位: 中国科学院

国际统一刊号: ISSN 1674-1056

主办单位: 中国物理学会和中国科学院物理研究所

国内统一刊号: CN 11-5639/O4

编 辑: Chinese Physics B 编辑部

编辑部地址: 北京 中关村 中国科学院物理研究所内

出 版: 中国物理学会

通信地址: 100190 北京 603 信箱

出版日期: 2024年1月

电 话: (010) 82649026, 82649519

印刷装订: 北京科信印刷有限公司

传 真: (010) 82649027

国内发行: Chinese Physics B 编辑部

“Chinese Physics B”网址:

国外发行: IOP Publishing Ltd

<http://cpb.iphy.ac.cn>

发行范围: 公开发行

<http://iopscience.iop.org/journal/1674-1056>

Advisory Board

Chen Jia-Er(陈佳洱), T. D. Lee(李政道), Samuel C. C. Ting(丁肇中), C. N. Yang(杨振宁), Wang Nai-Yan(王乃彦), Zhao Zhong-Xian(赵忠贤), Yang Guo-Zhen(杨国桢)

Editorial Board

Editor-in-Chief

Gao Hong-Jun(高鸿钧)

Chinese Academy of Sciences, China

Associate Editors

Chen Xian-Hui(陈仙辉)

University of Science and Technology of China, China

Fan Heng(范桁)

Institute of Physics, Chinese Academy of Sciences, China

Gao Yuan-Ning(高原宁)

Peking University, China

Li Jian-Xin(李建新)

Nanjing University, China

Li Ru-Xin(李儒新)

Shanghai Tech University, China

Ma Yan-Ming(马琰铭)

Jilin University, China

Ouyang Zhong-Can(欧阳钟灿)	Institute of Theoretical Physics, Chinese Academy of Sciences, China
Shen Bao-Gen(沈保根)	Institute of Physics, Chinese Academy of Sciences, China
Wang Wei-Hua(汪卫华)	Institute of Physics, Chinese Academy of Sciences, China
Wang Zi-Qiang(汪自强)	Boston College USA
Wang Ning(王宁)	The Hong Kong University of Science & Technology, China
Xiong Qi-Hua(熊启华)	Tsinghua University, China
Yao Wang(姚望)	The University of Hong Kong, China
Zhang Jie(张杰)	Chinese Physical Society, China
Zhang Yuan-Bo(张远波)	Fudan University, China

Editorial Board

Chen Chong-Lin(陈充林)	University of Texas at San Antonio, USA
Chen Wei(陈伟)	National University of Singapore, Singapore
Chen Xiao-Song(陈晓松)	Beijing Normal University, China
Chen Yu-Ao(陈宇翱)	University of Science and Technology of China, China
Cheng Jian-Chun(程建春)	Nanjing University, China
Cheng Meng(程蒙)	Yale University, USA
Cui Xiao-Dong(崔晓冬)	The University of Hong Kong, China
Dai Qing(戴庆)	National Center for Nanoscience and Technology, China
Ding Da-Jun(丁大军)	Jilin University, China
Fang Zhong(方忠)	Institute of Physics, Chinese Academy of Sciences, China
Feng Shi-Ping(冯世平)	Beijing Normal University, China
Feng Xin-Liang(冯新亮)	Dresden University of Technology, Germany
Gao Wei-Bo(高炜博)	Nanyang Technological University, Singapore
Gong Xin-Gao(龚新高)	Fudan University, China
Gu Chang-Zhi(顾长志)	Institute of Physics, Chinese Academy of Sciences, China
Guo Hong(郭鸿)	McGill University, Canada
Hu Xiao(胡晓)	National Institute for Materials Science, Japan
Huang Xue-Jie(黄学杰)	Institute of Physics, Chinese Academy of Sciences, China
Ji Wei(季威)	Renmin University of China, China
Jia Jin-Feng(贾金锋)	Shanghai Jiao Tong University, China
Jiang Ying(江颖)	Peking University, China
Leong Chuan Kwek	National University of Singapore, Singapore
Lei Dangyuan(雷党愿)	City University of Hong Kong, China
Li Bao-Wen(李保文)	University of Colorado Boulder, USA
Li Jian-Qi(李建奇)	Institute of Physics, Chinese Academy of Sciences, China
Li Xiao-Guang(李晓光)	University of Science and Technology of China, China
Liu Bing-Bing(刘冰冰)	Jilin University, China
Liu Chao-Xing(刘朝星)	Pennsylvania State University, USA
Liu Xiang-Yang(刘向阳)	Xiamen University, China
Liu Yi-Chun(刘益春)	Northeast Normal University, China
Liu Zheng(刘政)	Nanyang Technological University, Singapore
Long Gui-Lu(龙桂鲁)	Tsinghua University, China
Lu Zheng-Tian(卢征天)	University of Science and Technology of China, China
Lu Dong-Hui(路东辉)	Stanford Synchrotron Radiation Lightsource, SLAC National Accelerator Laboratory, USA
Lu Wei(陆卫)	Shanghai Institute of Technical Physics, Chinese Academy of Sciences, China
Luo Hong-Gang(罗洪刚)	Lanzhou University, China
Lu Guang-Hong(吕广宏)	Beihang University, China
Lu Li(吕力)	Institute of Physics, Chinese Academy of Sciences, China

Ma Xu-Cun(马旭村)	Tsinghua University, China
Ma Yu-Gang(马余刚)	Fudan University, China
Ni Pei-Gen(倪培根)	National Natural Science Foundation of China, China
Niu Qian(牛谦)	University of Texas, USA
Ouyang Qi(欧阳颀)	Peking University, China
Pan Yi(潘毅)	Xi'an Jiaotong University, China
Shen De-Zhen(申德振)	Changchun Institute of Optics, Fine Mechanics and Physics, Chinese Academy of Sciences, China
Shen Ze-Xiang(申泽骧)	Nanyang Technological University, Singapore
Shen Jian(沈健)	Fudan University, China
Si Qi-Miao(斯其苗)	Rice University, USA
Sun Chang-Pu(孙昌璞)	Beijing Computational Science Research Center, China
Sun Xiao Wei(孙小卫)	Southern University of Science and Technology, China
Tian Yong-Jun(田永君)	Yanshan University, China
Tong Li-Min(童利民)	Zhejiang University, China
John S. Tse	University of Saskatchewan, Canada
Wan Bao-Nian(万宝年)	Institute of Plasma Physics, Chinese Academy of Sciences, China
Wang Bo-Gen(王伯根)	Nanjing University, China
Wang Kai-You(王开友)	Institute of Semiconductors, Chinese Academy of Sciences, China
Wang Wei(王炜)	Nanjing University, China
Wang Ya-Yu(王亚愚)	Tsinghua University, China
Wang Yu-Peng(王玉鹏)	Institute of Physics, Chinese Academy of Sciences, China
Wei Su-Huai(魏苏淮)	Beijing Computational Science Research Center, China
Wen Wei-Jia(温维佳)	The Hong Kong University of Science & Technology, China
Wen Hai-Hu(闻海虎)	Nanjing University, China
Wu Nan-Jian(吴南健)	Institute of Semiconductors, Chinese Academy of Sciences, China
Xiang Tao(向涛)	Institute of Physics, Chinese Academy of Sciences, China
Xiao Di(肖迪)	Carnegie Mellon University, USA
Xie Xin-Cheng(谢心澄)	Peking University, China
Xu Hong-Xing(徐红星)	Wuhan University, China
Xu Zhi-Chuan(徐志川)	Nanyang Technological University, Singapore
Xu Xiao-Dong(许晓栋)	University of Washington, USA
Yang Guo-Wei(杨国伟)	Sun Yat-Sen University, China
Yang Lan(杨兰)	Washington University in St. Louis, USA
Ye Jun(叶军)	University of Colorado, USA
Zhang Fu-Chun(张富春)	University of Chinese Academy of Sciences, China
Zhang Hong(张红)	Sichuan University, China
Zhang Yong(张勇)	The University of North Carolina at Charlotte, USA
Zhang Zhen-Yu(张振宇)	University of Science and Technology of China, China
Zhao Hong-Wei(赵红卫)	Institute of Modern Physics, Chinese Academy of Sciences, China
Zhao Hui(赵辉)	The University of Kansas, USA
Zhao Wei-Juan(赵维娟)	Zhengzhou University, China
Zheng Zhi-Gang(郑志刚)	Huaqiao University, China
Zhou Wu(周武)	University of Chinese Academy of Sciences, China
Zhou Xin(周昕)	University of Chinese Academy of Sciences, China
Zhou Xin(周欣)	Wuhan Institute of Physics and Mathematics, Chinese Academy of Sciences, China
Zhou Xing-Jiang(周兴江)	Institute of Physics, Chinese Academy of Sciences, China
Zhu Bang-Fen(朱邦芬)	Tsinghua University, China

Editorial Staff

Wang Jiu-Li(王久丽) (Editorial Director) Cai Jian-Wei(蔡建伟) Zhai Zhen(翟振)

Scheme of negative acoustic radiation force based on a multiple-layered spherical structure

Menyang Gong(宫门阳)¹, Xin Xu(徐鑫)¹, Yupei Qiao(乔玉配)²,
Jiehui Liu(刘杰惠)¹, Aijun He(何爱军)³, and Xiaozhou Liu(刘晓宙)^{1,4,†}

¹Key Laboratory of Modern Acoustics, Institute of Acoustics and School of Physics,
Collaborative Innovation Center of Advanced Microstructures, Nanjing University, Nanjing 210093, China

²School of Physics and Electronic Science, Guizhou Normal University, Guiyang 550001, China

³School of Electronic Science and Engineering, Nanjing University, Nanjing 210023, China

⁴State Key Laboratory of Acoustics, Institute of Acoustics, Chinese Academy of Sciences, Beijing 100190, China

(Received 1 August 2023; revised manuscript received 7 September 2023; accepted manuscript online 18 September 2023)

Acoustic radiation force (ARF), as an important particle manipulation method, has been extensively studied in recent years. With the introduction of the concept of “acoustic tweezers”, negative acoustic radiation has become a research hotspot. In this paper, a scheme of realizing negative ARF based on the multiple-layered spherical structure design is proposed. The specific structure and design idea are presented. Detailed theoretical calculation analysis is carried out. Numerical simulations have been performed to verify the correctness of this prediction. The conjecture that the suppression of backscattering can achieve negative ARF is verified concretely, which greatly expands the application prospect and design ideas of the ARF. This work has laid a theoretical foundation for realizing precise control of the structure.

Keywords: acoustic tweezers, negative acoustic radiation force, particle manipulation

PACS: 43.25.Qp, 43.35.Wa, 43.80.Gx

DOI: [10.1088/1674-1056/acfa80](https://doi.org/10.1088/1674-1056/acfa80)

1. Introduction

Ashkin proposed the concept of “optical tweezers” to achieve precise manipulation of microscopic particles, and therefore won the Nobel Prize in 2018. To overcome the shortcomings of optical tweezers in terms of scale and thermal effect,^[1] Wu proposed “acoustic tweezers” based on acoustic radiation force (ARF).^[2] Some ideas for building acoustic tweezers have gradually been proposed.^[3–5] The generation of ARF is based on the nonlinear effect of the sound field. Through this effect, the momentum and angular momentum transfer can be realized between the sound field and the particles. Compared with the traditional particle manipulation method, ARF has a very significant advantage: The manipulation process is non-contact. Therefore, the ARF has gained extensive attention and wide application in ultrasound medicine and particle control. The research and investigation of the law of ARF are of great important significance. The ARF of standard particles such as cylindrical particles and spherical particles in the plane wave field or Bessel beams has been studied in detail.^[1,2,6–16] The effects of ARF on particles in viscous media have also been included in the investigations.^[17] ARFs with normal closed boundaries have been studied.^[18,19] The ARF of standard particles in non-diffracted waves has also been investigated.^[20] Resonant adhesion structure has been studied to make negative ARF.^[21] Based on the angular spectrum and multipole expansion, the calculation meth-

ods of acoustic radiation force and moment have been further developed.^[22,23] The sound field of the spherical shell structure has been analyzed and proved to be a meaningful attempt.^[24–27] Some schemes of manipulating particles are carried out by using acoustic streaming.^[28–30] In the field of acoustic manipulations, some of important progress have been made.^[31–33] Recently, the influence of cavity and interface on ARF has been evaluated.^[34–36]

The concept of “acoustic tweezers” emphasizes the construction of acoustic potential wells for particle manipulation and trapping. In actual scenes, the sound source is often confined to a small angle relative to the particles. Therefore, it is of great significance to realize the negative ARF based on a unidirectional or small-angle sound beam. However, based on the definition, the negative ARF represents that the structure in the sound field is subjected to a force towards the sound source, which is extraordinary and difficult to achieve by traditional methods. Gong *et al.*^[37] previously proposed a solution to the negative ARF of a single acoustic beam based on non-diffracted waves. In the calculation of the Bessel beam, Marston mentioned that based on the suppression of backscatter, it is possible to realize the negative ARF.^[38] The first numerical demonstration of the negative ARF by suppressing the backscattering of non-spherical objects was performed by Gong *et al.*^[39] Therefore, in this work, the design of suppressing the backscattering of the controlled structure

[†]Corresponding author. E-mail: xzliu@nju.edu.cn

is considered to explore the possibility of the negative ARF of the unidirectional sound beam acting on the structure. The sound field analysis of core–shell particles has been analyzed by Leibacher *et al.*^[40] In this paper, the structure is designed to achieve suppression of backscattering. After a lot of parameter verifications and numerical simulations, a structure that exhibits negative ARF effects in a specific frequency spectrum has been successfully found. This demonstrates the feasibility of achieving negative ARF by suppressing backscattering.

2. Analysis of multi-layered spherical structure

Due to the limitations of most practical application scenarios, the structure design needs to be as independent as possible from the angle parameter and only related to the radial coordinates. Majid Rajabi *et al.* achieved acoustic radiation force control by pulsating spherical carriers in 2017,^[41] which has been proved as an effective way. Therefore, the use of a multi-layered spherical structure to design the distribution of acoustic parameters is considered.

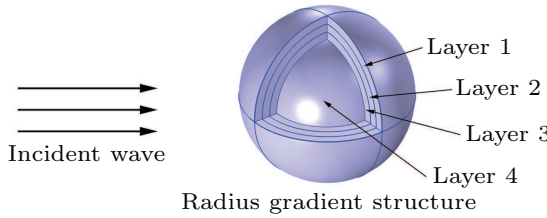


Fig. 1. Discrete multi-layered spherical structure in sound field. The source is a unidirectional monochromatic wave.

In the design and implementation process, the multiple-layered structure is generally described in a differential manner. Therefore, in calculations, the multiple-layered structure is discretized into a multiple-layered spherical shell as shown in Fig. 1. All kinds of unidirectional sound beams can be expanded into a linear combination of plane waves. Therefore, the incident beam considered in the calculation is a plane wave. Since the multi-layer spherical shell structure subjected to radiation force is a spherical symmetrical structure, the plane wave can be expanded in spherical coordinates. Since ARF calculation will be time-averaged, the frequency domain expression is used. Incident wave Φ_i can be expressed as follows:

$$\Phi_i = \sum_{k_0} \Phi_{k_0} \sum_{n=0}^{\infty} (2n+1)(i)^n j_n(k_0 r) P_n(\cos \theta), \quad (1)$$

where Φ_{k_0} is the incident velocity potential, k_0 is the wavenumber of the sound wave in the external environment medium, j_n is the first kind of spherical Bessel function of order n , P_n is the Legendre function of order n .

Similarly, the scattered wave Φ_s can also be expanded into a linear combination of spherical waves

$$\Phi_s = \sum_{k_0} \Phi_{k_0} \sum_{n=0}^{\infty} A_{n,s} (2n+1)(i)^n h_n^{(1)}(k_0 r) P_n(\cos \theta), \quad (2)$$

where $A_{n,s}$ is the coefficient of scattered sound wave, $h_n^{(1)}$ is the Hankle function of the first kind of order n .

Therefore, the total sound field sound pressure Φ_0 in the environmental medium can be expressed as

$$\Phi_0 = \Phi_i + \Phi_s = \sum_{k_0} \Phi_{k_0} \sum_{n=0}^{\infty} (2n+1)(i)^n [j_n(k_0 r) + A_{n,s} h_n^{(1)}(k_0 r)] P_n(\cos \theta). \quad (3)$$

For the reason that the sound wave needs to propagate to the interior of the controlled structure, the elastic boundary conditions should be taken between the medium and the structure, and between the middle and layers of the structure. There is mode conversion at the boundary, so the medium particle displacement satisfies the Navier equation

$$\nabla^2 u + \frac{\lambda + \mu}{\mu} \frac{\partial}{\partial t} \nabla(\nabla \cdot u) = \frac{1}{c_s^2} \frac{\partial^2 u}{\partial t^2}, \quad (4)$$

here λ and μ are the Lami coefficient, $c_s = \sqrt{\mu/\rho_0}$.

Because the boundary conditions are described by velocity continuity, the internal sound field is also described by velocity potential to unify the expression. Since the sound field will form a stable sound field structure after incident for a period of time, it is only necessary to sort out the general form of velocity potential expression, and obtain the undetermined parameters by boundary conditions in the form of undetermined coefficients.

For the first layer of medium, the velocity potential of longitudinal wave can be expressed as

$$\Phi_1 = \sum_k \Phi_{k_0} \sum_{n=0}^{\infty} (2n+1)(i)^n [A_{n,1a} j_n(k_{11} r) + A_{n,1b} n_n(k_{11} r)] P_n(\cos \theta), \quad (5)$$

here Φ_{k_0} is velocity potential constant, n_n is Neumann function, $A_{n,1a}$ and $A_{n,1b}$ are pending parameters, k_{11} is the longitudinal wavenumber in the spherical layer 1.

The transverse wave velocity potential

$$\Psi_1 = \sum_k \Phi_{k_0} \sum_{n=0}^{\infty} (2n+1)(i)^n [A_{n,1c} j_n(k_{12} r) + A_{n,1d} n_n(k_{12} r)] \frac{dP_n(\cos \theta)}{d\theta}. \quad (6)$$

Similarly, for the velocity potential in the q -th layer, longitudinal wave velocity potential:

$$\Phi_q = \sum_k \Phi_{k_0} \sum_{n=0}^{\infty} (2n+1)(i)^n [A_{n,q a} j_n(k_{q1} r) + A_{n,q b} n_n(k_{q1} r)] P_n(\cos \theta), \quad (7)$$

then transverse wave velocity potential

$$\Psi_q = \sum_k \Phi_{k0} \sum_{n=0}^{\infty} (2n+1)(i)^n \times [A_{n,qc} j_n(k_{q2}r) + A_{n,qd} n_n(k_{q2}r)] \frac{dP_n(\cos \theta)}{d\theta}, \quad (8)$$

where $A_{n,qa}$, $A_{n,qb}$, $A_{n,qc}$, and $A_{n,qd}$ are pending parameters, k_{q1} and k_{q2} are the longitudinal wavenumber and transverse wavenumber in the q -th spherical shell individually. If the q -th layer is the innermost layer, the Neumann function item returns to zero, and the velocity potential in the q -th spherical shell is given below.

The longitudinal wave velocity potential can be written as

$$\Phi = \sum_k \Phi_{k0} \sum_{n=0}^{\infty} (2n+1)(i)^n A_{n,qa} j_n(k_{q1}r) P_n(\cos \theta). \quad (9)$$

The transverse wave velocity potential can be written as

$$\Psi = \sum_k \Phi_{k0} \sum_{n=0}^{\infty} (2n+1)(i)^n A_{n,qc} j_n(k_{q2}r) \frac{dP_n(\cos \theta)}{d\theta}. \quad (10)$$

For the discretized multi-layered spherical structure of m layer, there are $4(m-1)+3=4m-1$ independent boundary condition equations, and $4m+1-2=4m-1$ undetermined coefficients need to be determined. Therefore, this system of equations is mathematically solvable. Then, the boundary conditions of this structure will be analyzed in detail.

The specific continuity equations and the expansion of the corresponding parameters are given below.

(i) Boundary conditions between the first layer structure and the external medium

The normal displacement continuity:

$$u_{r0} = \frac{\partial \Phi_0}{\partial r} + \frac{1}{r \sin \theta} \frac{\partial \Psi_0}{\partial \theta} = \frac{\partial (\Phi_i + \Phi_s)}{\partial r},$$

$$\begin{aligned} \sigma_{r,q} &= 2\mu \frac{\partial u_{r,q}}{\partial r} + \lambda (\nabla \cdot u_q) = (2\mu + \lambda) \left(\frac{\partial^2 \Phi_q}{\partial r^2} + \frac{1}{r \sin \theta} \frac{\partial^2 \Psi_q}{\partial r \partial \theta} - \frac{1}{r^2 \sin \theta} \frac{\partial \Psi_q}{\partial \theta} \right) + \lambda \left(\frac{1}{r} \frac{\partial^2 \Phi_q}{\partial \theta^2} - \frac{1}{r} \frac{\partial \Psi_q}{\partial \theta} - \frac{\partial^2 \Psi_q}{\partial \theta \partial r} \right), \\ \sigma_{r,q+1} &= 2\mu \frac{\partial u_{r,q+1}}{\partial r} + \lambda (\nabla \cdot u_{q+1}) \\ &= (2\mu + \lambda) \left(\frac{\partial^2 \Phi_{q+1}}{\partial r^2} + \frac{1}{r \sin \theta} \frac{\partial^2 \Psi_{q+1}}{\partial r \partial \theta} - \frac{1}{r^2 \sin \theta} \frac{\partial \Psi_{q+1}}{\partial \theta} \right) + \lambda \left(\frac{1}{r} \frac{\partial^2 \Phi_{q+1}}{\partial \theta^2} - \frac{1}{r} \frac{\partial \Psi_{q+1}}{\partial \theta} - \frac{\partial^2 \Psi_{q+1}}{\partial \theta \partial r} \right), \\ \sigma_{r,q}(r_{q,q+1}) &= \sigma_{r,q+1}(r_{q,q+1}). \end{aligned} \quad (15)$$

The tangential stress continuity:

$$\begin{aligned} \sigma_{\theta,q} &= \mu \left(\frac{1}{r} \frac{\partial u_{r,q}}{\partial \theta} + \frac{\partial u_{\theta,q}}{\partial r} - \frac{u_{\theta,q}}{r} \right) = \frac{\mu}{r} \left[2 \frac{\partial^2 \Phi_q}{\partial r \partial \theta} + \frac{1}{r \sin \theta} \frac{\partial^2 \Psi_q}{\partial \theta^2} - \frac{\cos \theta}{r \sin \theta^2} \frac{\partial \Psi_q}{\partial \theta} - \frac{2}{r} \frac{\partial \Phi_q}{\partial \theta} + \frac{2}{r} \Psi_q - r \frac{\partial^2 \Psi_q}{\partial r^2} \right], \\ \sigma_{\theta,q+1} &= \mu \left(\frac{1}{r} \frac{\partial u_{r,q+1}}{\partial \theta} + \frac{\partial u_{\theta,q+1}}{\partial r} - \frac{u_{\theta,q+1}}{r} \right) \\ &= \frac{\mu}{r} \left[2 \frac{\partial^2 \Phi_{q+1}}{\partial r \partial \theta} + \frac{1}{r \sin \theta} \frac{\partial^2 \Psi_{q+1}}{\partial \theta^2} - \frac{\cos \theta}{r \sin \theta^2} \frac{\partial \Psi_{q+1}}{\partial \theta} - \frac{2}{r} \frac{\partial \Phi_{q+1}}{\partial \theta} + \frac{2}{r} \Psi_{q+1} - r \frac{\partial^2 \Psi_{q+1}}{\partial r^2} \right], \\ \sigma_{\theta,q}(r_{q,q+1}) &= \sigma_{\theta,q+1}(r_{q,q+1}), \end{aligned} \quad (16)$$

$$\begin{aligned} u_{r1} &= \frac{\partial \Phi_1}{\partial r} + \frac{1}{r \sin \theta} \frac{\partial \Psi_1}{\partial \theta}, \\ u_{r0} &= u_{r1}. \end{aligned} \quad (11)$$

The normal stress continuity:

$$\begin{aligned} \sigma_{r0} &= (2\mu + \lambda) \frac{\partial^2 \Phi_0}{\partial r^2} + \lambda \frac{\partial^2 \Phi_0}{\partial r \partial \theta} \\ &= (2\mu + \lambda) \frac{\partial^2 (\Phi_i + \Phi_s)}{\partial r^2} + \lambda \frac{\partial^2 (\Phi_i + \Phi_s)}{\partial r \partial \theta}, \\ \sigma_{r1} &= 2\mu \frac{\partial u_r}{\partial r} + \lambda (\nabla \cdot u) \\ &= (2\mu + \lambda) \left(\frac{\partial^2 \Phi_1}{\partial r^2} - \frac{1}{r^2 \sin \theta} \frac{\partial \Psi_1}{\partial \theta} + \frac{1}{r \sin \theta} \frac{\partial^2 \Psi_1}{\partial \theta \partial r} \right) \\ &\quad + \lambda \left(\frac{\partial^2 \Phi_1}{\partial r \partial \theta} + \frac{-\cos \theta}{r \sin^2 \theta} \frac{\partial \Psi_1}{\partial \theta} + \frac{1}{r \sin \theta} \frac{\partial^2 \Psi_1}{\partial \theta^2} \right), \\ \sigma_{r0} &= \sigma_{r1}, \end{aligned} \quad (12)$$

where Φ is the velocity potential of the longitudinal wave and Ψ is the velocity potential of the transverse wave.

(ii) Boundary conditions between the q -th layer structure and the $(q+1)$ -th layer structure

The normal displacement continuity:

$$\begin{aligned} u_{r,q} &= \frac{\partial \Phi_q}{\partial r} + \frac{1}{r \sin \theta} \frac{\partial \Psi_q}{\partial \theta}, \\ u_{r,q+1} &= \frac{\partial \Phi_{q+1}}{\partial r} + \frac{1}{r \sin \theta} \frac{\partial \Psi_{q+1}}{\partial \theta}, \\ u_{r,q}(r_{q,q+1}) &= u_{r,q+1}(r_{q,q+1}). \end{aligned} \quad (13)$$

The tangential displacement continuity:

$$\begin{aligned} u_{\theta,q} &= \frac{1}{r} \frac{\partial \Phi_q}{\partial \theta} - \frac{1}{r} \frac{\partial (r \Psi_q)}{\partial r}, \\ u_{\theta,q+1} &= \frac{1}{r} \frac{\partial \Phi_{q+1}}{\partial \theta} - \frac{1}{r} \frac{\partial (r \Psi_{q+1})}{\partial r}, \\ u_{\theta,q}(r_{q,q+1}) &= u_{\theta,q+1}(r_{q,q+1}). \end{aligned} \quad (14)$$

The normal stress continuity:

$$\begin{aligned} \sigma_{r,q} &= 2\mu \frac{\partial u_{r,q}}{\partial r} + \lambda (\nabla \cdot u_q) = (2\mu + \lambda) \left(\frac{\partial^2 \Phi_q}{\partial r^2} + \frac{1}{r \sin \theta} \frac{\partial^2 \Psi_q}{\partial r \partial \theta} - \frac{1}{r^2 \sin \theta} \frac{\partial \Psi_q}{\partial \theta} \right) + \lambda \left(\frac{1}{r} \frac{\partial^2 \Phi_q}{\partial \theta^2} - \frac{1}{r} \frac{\partial \Psi_q}{\partial \theta} - \frac{\partial^2 \Psi_q}{\partial \theta \partial r} \right), \\ \sigma_{r,q+1} &= 2\mu \frac{\partial u_{r,q+1}}{\partial r} + \lambda (\nabla \cdot u_{q+1}) \\ &= (2\mu + \lambda) \left(\frac{\partial^2 \Phi_{q+1}}{\partial r^2} + \frac{1}{r \sin \theta} \frac{\partial^2 \Psi_{q+1}}{\partial r \partial \theta} - \frac{1}{r^2 \sin \theta} \frac{\partial \Psi_{q+1}}{\partial \theta} \right) + \lambda \left(\frac{1}{r} \frac{\partial^2 \Phi_{q+1}}{\partial \theta^2} - \frac{1}{r} \frac{\partial \Psi_{q+1}}{\partial \theta} - \frac{\partial^2 \Psi_{q+1}}{\partial \theta \partial r} \right), \\ \sigma_{r,q}(r_{q,q+1}) &= \sigma_{r,q+1}(r_{q,q+1}). \end{aligned} \quad (15)$$

where, $u_{r,q}$ is the radial component of the particle vibration velocity in layer q , $u_{\theta,q}$ is the angular component of the particle vibration velocity in layer q , Φ_q is the longitudinal velocity potential in layer q , Ψ_q is the transverse velocity potential in layer q . To determine the undetermined coefficients, we organize them into a matrix solution: $A_N = A_{1N}/A_{2N}$. For m-storey structure, both matrices are $(4m - 1) \times (4m - 1)$ matrices. The specific expression of the matrix is shown in the appendix.

Thus, the velocity potential field information scattered by the multi-layered spherical structure is obtained. Based on definition, the expression of the ARF on the multi-layered spherical structure can be expressed as

$$\begin{aligned} \mathbf{F} &= \iint_s (p - p_0) \mathbf{n} ds \\ &= \iint_s \rho_0 \left(\sum_k i k c_0 \Phi_0 \right) \mathbf{n} ds + \iint_s \frac{1}{2} \rho_0 \left(\frac{\partial \Phi_0}{\partial z} \right)^2 \mathbf{n} ds \\ &\quad - \iint_s \frac{1}{2} \frac{\rho_0}{c^2} \left(\sum_k i k c_0 \Phi_0 \right)^2 \mathbf{n} ds, \end{aligned} \quad (17)$$

where z is the propagation direction of the incident sound beam and s is the surface of the geometrical surface of the particles.

Based on Eqs. (1)–(16), the velocity potential distribution of the entire sound field can be obtained by means of undetermined coefficients. Then the total velocity potential Φ_0 in the external medium can be obtained by Eq. (3). The integral in Eq. (17) including the total velocity potential Φ_0 in the external medium is implemented by accumulating the discretized velocity potentials. The expression of the total velocity potential Φ_0 includes the position coordinates, which could be further simplified based on symmetry during the accumulation process.

3. Finite element simulation of multi-layered spherical structure

In Section 2, the analytical expression of the ARF received by the multi-layered spherical structure in a unidirectional sound beam is obtained. After a large number of parameter verifications, we find that the specific multi-layered spherical structure can achieve the negative ARF in the unidirectional sound beam sound field. The following structures shown in Fig. 2–7 are aluminum–water–aluminum–water alternating multi-layered spherical structures. To further clarify the physical mechanism, as a control, the structures of copper–water–copper–water multi-layered spherical structure in Fig. 8 and 9 and PVC (polyvinyl chloride)–water–PVC–water multi-layered spherical structure in Figs. 10 and 11 are also verified. The relevant parameters are shown in Table 1.

To verify the real existence of back suppression in layered structure design, the finite element simulations based on

COMSOL Multiphysics 6.1 are carried out. In all finite element simulations, the radius R of the multiple-layered spherical structure is set to 0.5 mm. The incident background pressure is set to 1 Pa. The maximum grid size is set to 1/6 of the wavelength, so the sound field distribution could be accurate enough. By means of finite element simulation, the velocity potential distribution of the entire sound field is obtained. Based on the definition formula for the calculation of the ARF Eq. (17), the ARF on the structure can be obtained by performing the corresponding integral on the outside of the controlled structure surface. In the actual calculations, the probe tool of the finite element simulation is applied, and the velocity potential containing the position coordinates is uniformly sampled. With sufficiently dense sampling, the integral is calculated by accumulation, and the differential is calculated by difference method. In practice, this process can be further simplified by symmetry. For example, based on the rotational symmetry of the structure, only the component integration of the ARF in the incident direction of the incident acoustic beam is required. The blue square point in Figs. 2, 3, 4, 8 and 10 is obtained due to the frequency sweep of finite element analysis, and the black curve is drawn based on the analytical solution in Section 2. The finite element simulations are carried out in three dimensions. Figures 5–7, 9, 11 are sections through the propagation direction. The innermost hierarchical structure is the multiple-layered spherical structure shown in Fig. 1. Due to symmetry, all sound pressure distributions have been shown. The outer dark blue layer in Figs. 5–7, 9, 11 is the perfectly-matched layer. The perfectly-matching layer is far enough from the controlled structure to perfectly absorb the sound wave without affecting the distribution of the sound field. It can be seen from the figures that the points obtained by finite element analysis basically fall on the curve of analytical solution, which also confirms the correctness of finite element simulation and analytical solution.

Table 1. Parameters selections.

Parameter	Symbols	Numerical value
Sound velocity of medium	c_0	1500 m/s
Density of medium	ρ_0	1000 kg/m ³
Longitudinal sound velocity of aluminum	c_{al}	6320 m/s
Transverse sound velocity of aluminum	c_{at}	2600 m/s
Density of aluminum	ρ_a	2700 kg/m ³
Longitudinal sound velocity of copper	c_{cl}	4720 m/s
Transverse sound velocity of copper	c_{ct}	2350 m/s
Density of copper	ρ_c	8960 kg/m ³
Longitudinal Sound velocity of PVC	c_{PVC1}	2388 m/s
Transverse sound velocity of PVC	c_{PVCt}	1540 m/s
Density of PVC	ρ_{PVC}	1760 kg/m ³

Firstly, the four-layer structure of 1 : 3 : 1 : 5 is analyzed, and the parameter values are: $R_{layer1} = R/10$, $R_{layer2} = 3R/10$,

$R_{\text{layer}3} = R/10$. the schematic diagram of the variation of ARF with the spectrum is shown in Fig. 2. It could be seen that this structure can show obvious negative ARF when subjected to a single sound beam from 0.1 MHz to 3.5 MHz.

For a comparison, as shown in Fig. 3, the four-layer structure of $1 : 1 : 1 : 7$ is analyzed, and the parameter values are: $R_{\text{layer}1} = R/10$, $R_{\text{layer}2} = R/10$, $R_{\text{layer}3} = R/10$, the schematic diagram of the variation of ARF with the spectrum is shown in Fig. 3. We can see that this structure shows a narrow range negative ARF when subjected to a single acoustic beam from 0.1 MHz to 3.5 MHz.

Similarly, as shown in Fig. 4, the four-layer structure of $1 : 5 : 1 : 3$ is analyzed, and the parameter values are: $R_{\text{layer}1} = R/10$, $R_{\text{layer}2} = R/2$, $R_{\text{layer}3} = R/10$, the schematic diagram of the variation of ARF with the spectrum is shown in Fig. 4. We can see that this structure does not show negative ARF when subjected to a single sound beam from 0.1 MHz to 3.5 MHz.

The sound pressure distribution is equivalent to the distribution of the velocity potential. It can be seen from Eq. (17) that the velocity potential is an important factor that directly affects the ARF on the structure. In the previous conjecture proposed by Marston, the negative ARF can be obtained by suppressing backscattering.^[38] In Fig. 2, this conjecture is realized through a multi-layer spherical structure. In order to illustrate the process of backscattering suppression causing the reversal of ARF more vividly, the sound pressure distribution images based on several key frequency points are drawn. To analyze the mechanism of the generation and disappearance of negative ARF, the multiple-layered spherical structure and its surrounding sound field in the process of frequency scanning are drawn. The sound beam enters from left to right. It can be seen in Fig. 5 that when the structure is subjected to negative ARF, a strong scattering region is formed between the inner and outer layers of the structure, and the backscattering is obviously suppressed. Therefore, the structure is subjected to negative ARF. At low frequencies, the formation of this common vibration peak is not obvious, mainly manifested in the positive ARF. At high frequencies, the structure forms multiple scattering peaks, which counteract the effect of producing a scattering region that suppresses the backscattering peaks, and thus also exhibits positive ARFs.

In the four-layer structure of $1 : 1 : 1 : 7$ as shown in Fig. 6, the peak region of enhanced backscattering is formed synchronously in the process of forming the peak of inhibiting backscattering, and the inhibitory effect on backscattering is not obvious. Therefore, it only shows a narrow negative ARF range.

In the $1 : 5 : 1 : 3$ four-layer structure as shown in Fig. 7, other multiple scattering peaks are generated almost synchronously in the process of forming the peak of restraining

backscattering. Therefore, in this case, the particles are always subjected to positive ARF.

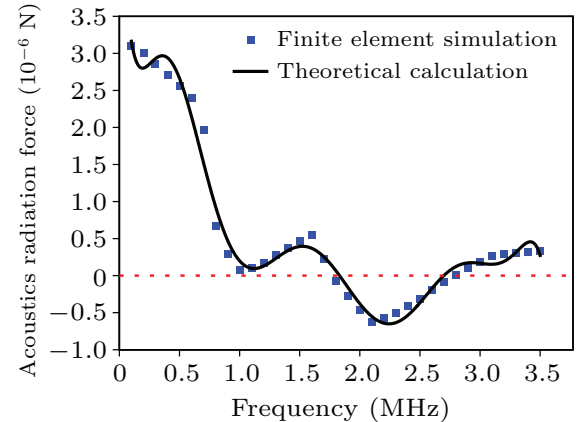


Fig. 2. The four-layer structure of $1 : 3 : 1 : 5$. $R_{\text{layer}1} = R/10$, $R_{\text{layer}2} = 3R/10$, $R_{\text{layer}3} = R/10$. The black solid line is the result of theoretical calculation. The blue point is the result of finite element simulation. The red dotted line is the reference line for the direction change of ARF. The structure is subjected to negative ARF in a specific frequency band.

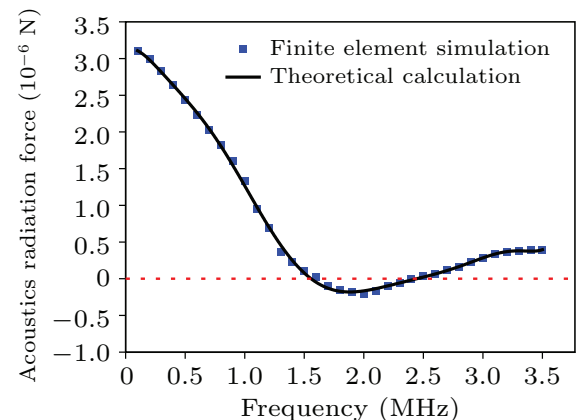


Fig. 3. The four-layer structure of $1 : 1 : 1 : 7$. $R_{\text{layer}1} = R/10$, $R_{\text{layer}2} = R/10$, $R_{\text{layer}3} = R/10$. The black solid line is the result of theoretical calculation. The blue point is the result of finite element simulation. The red dotted line is the reference line for the direction change of ARF. The structure shows a narrow range negative ARF.

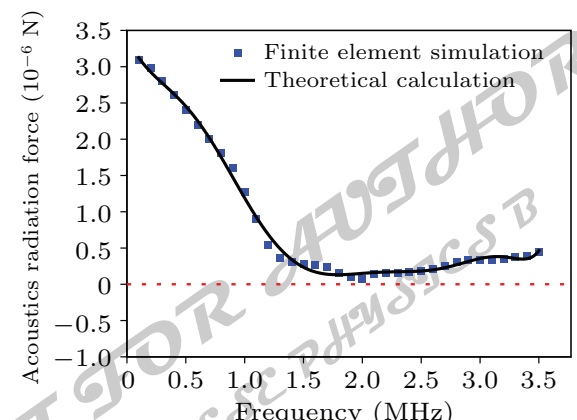


Fig. 4. The four-layer structure of $1 : 5 : 1 : 3$. $R_{\text{layer}1} = R/10$, $R_{\text{layer}2} = R/2$, $R_{\text{layer}3} = R/10$. The black solid line is the result of theoretical calculation. The blue point is the result of finite element simulation. The red dotted line is the reference line for the direction change of ARF. The structure shows no negative ARF.

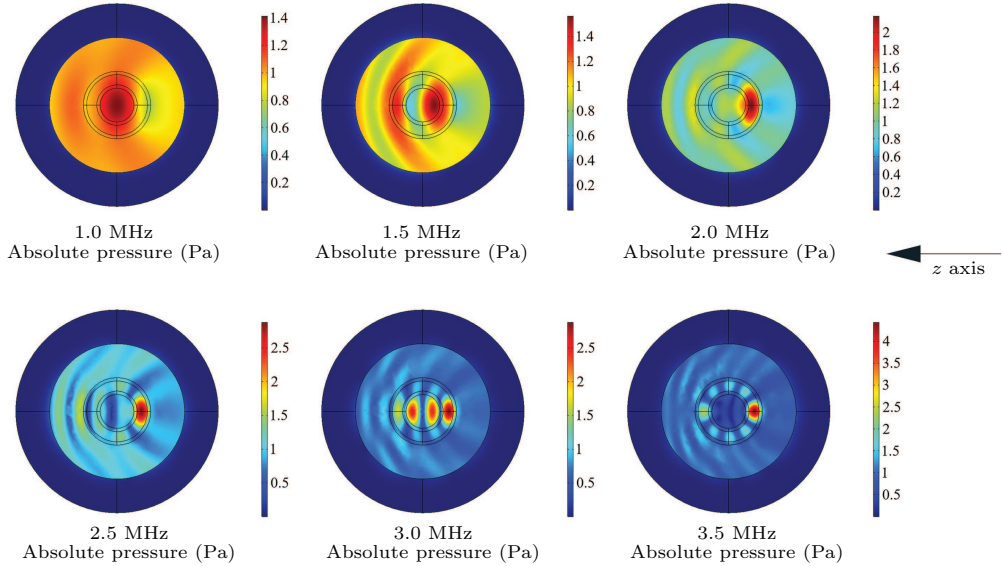


Fig. 5. Sound field distribution of multiple-layered spherical structure with four-layer of 1 : 3 : 1 : 5 incident by unidirectional monochromatic wave. The frequency points are 1.0 MHz, 1.5 MHz, 2.0 MHz, 2.5 MHz, 3.0 MHz, and 3.5 MHz respectively.

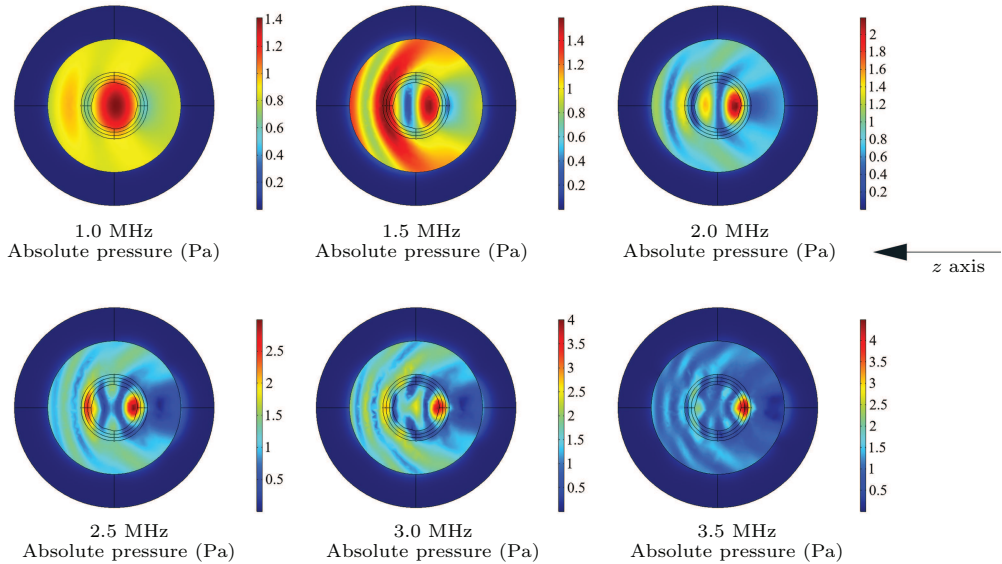


Fig. 6. Sound field distribution of multiple-layered spherical structure with four-layer of 1 : 1 : 1 : 7 incident by unidirectional monochromatic wave. The frequency points are 1.0 MHz, 1.5 MHz, 2.0 MHz, 2.5 MHz, 3.0 MHz, and 3.5 MHz respectively.

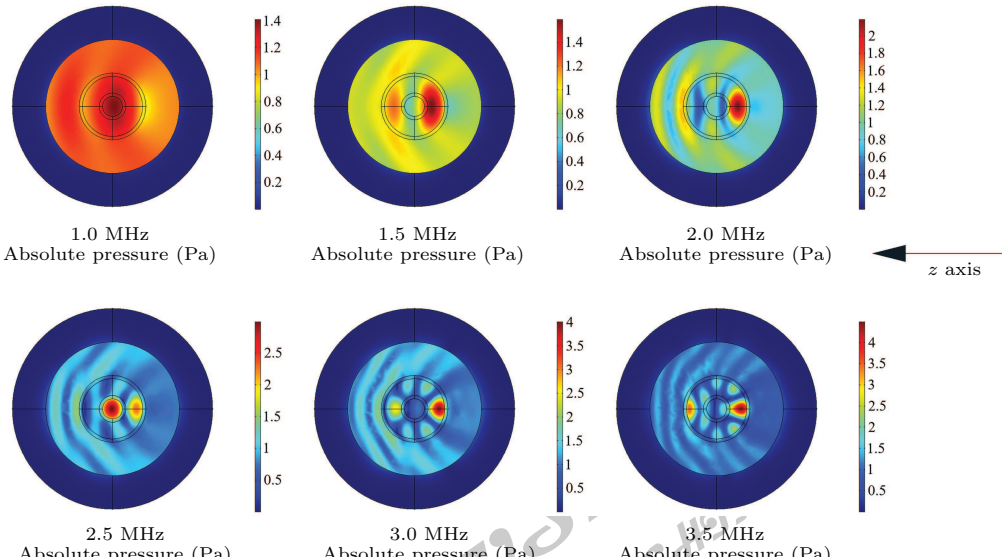


Fig. 7. Sound field distribution of multiple-layered spherical structure with four-layer of 1 : 5 : 1 : 3 incident by unidirectional monochromatic wave. The frequency points are 1.0 MHz, 1.5 MHz, 2.0 MHz, 2.5 MHz, 3.0 MHz, and 3.5 MHz respectively.

To further clarify the physical mechanism, the structures of copper–water–copper–water multiple-layered spherical structure of 1 : 3 : 1 : 5 is analyzed in Fig. 8, and the parameter values are: $R_{\text{layer}1} = R/10$, $R_{\text{layer}2} = 3R/10$, $R_{\text{layer}3} = R/10$. the schematic diagram of the variation of ARF with the spectrum is shown in Fig. 8. It could be seen that this structure shows no negative ARF.

Similarly, the copper–water–copper–water structure and its surrounding sound field in the process of frequency scanning are drawn in Fig. 9. It can be seen that in the interval where the suppression of backscattering should have occurred, the positive peak is generated synchronously. Therefore, only the minimum value of the positive ARF is generated, and there is no reversal of the direction of ARF.

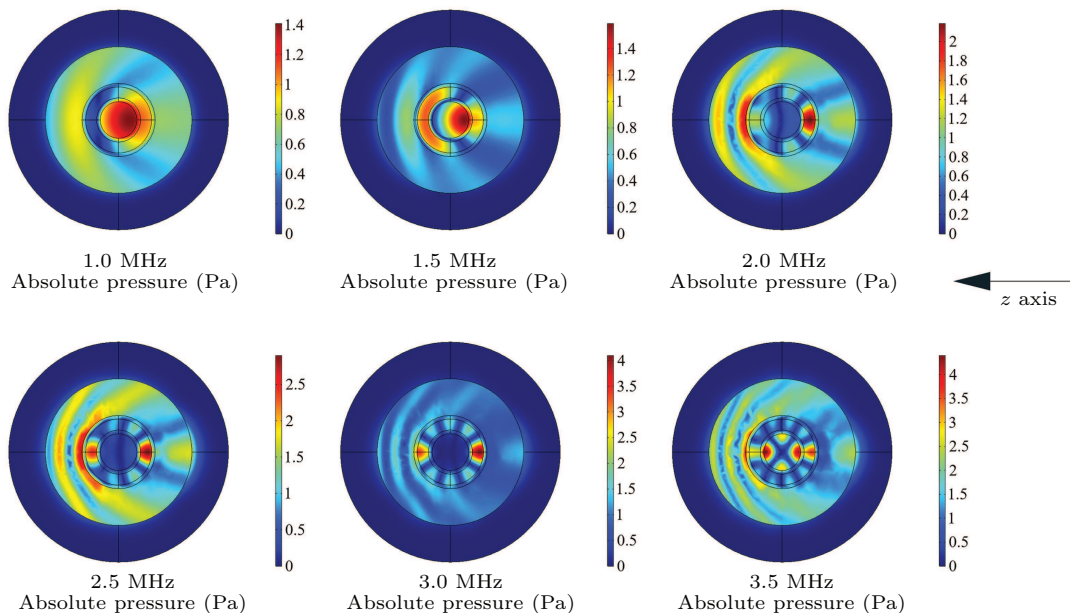


Fig. 9. Sound field distribution of copper–water–copper–water multiple-layered spherical structure with four-layer of 1 : 3 : 1 : 5 incident by unidirectional monochromatic wave. The frequency points are 1.0 MHz, 1.5 MHz, 2.0 MHz, 2.5 MHz, 3.0 MHz, and 3.5 MHz respectively.

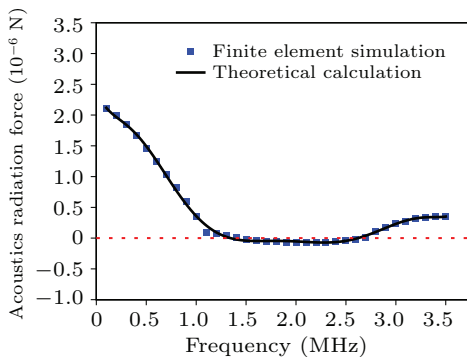


Fig. 10. The four-layer PVC–water–PVC–water structure of 1 : 3 : 1 : 5. $R_{\text{layer}1} = R/10$, $R_{\text{layer}2} = 3R/10$, $R_{\text{layer}3} = R/10$. The black solid line is the result of theoretical calculation. The blue point is the result of finite element simulation. The red dotted line is the reference line for the direction change of ARF. The structure shows insignificant negative ARF effects in a specific interval.

In addition to metal materials, the structure of organic materials has also been verified. The structures of PVC–water–PVC–water multiple-layered spherical structure of 1 : 3 : 1 : 5

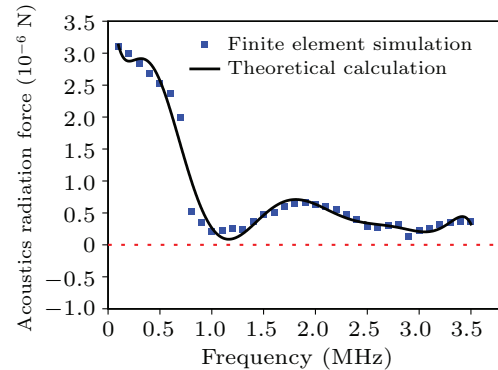
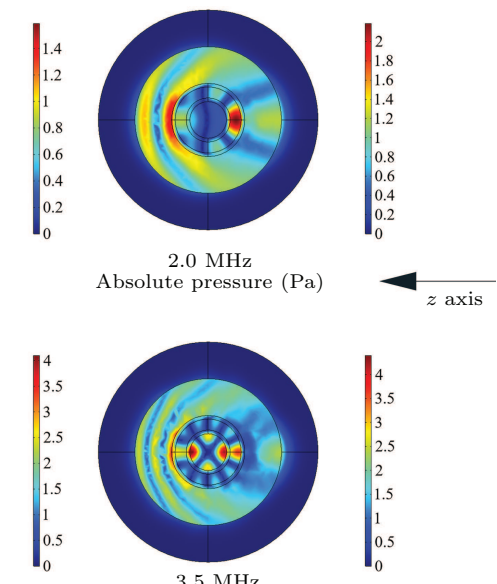


Fig. 8. The four-layer copper–water–copper–water structure of 1 : 3 : 1 : 5. $R_{\text{layer}1} = R/10$, $R_{\text{layer}2} = 3R/10$, $R_{\text{layer}3} = R/10$. The black solid line is the result of theoretical calculation. The blue point is the result of finite element simulation. The red dotted line is the reference line for the direction change of ARF. The structure shows no negative ARF.



is analyzed in Fig. 10, and the parameter value is: $R_{\text{layer}1} = R/10$, $R_{\text{layer}2} = 3R/10$, $R_{\text{layer}3} = R/10$. the schematic diagram of the variation of ARF with the spectrum is shown in Fig. 10. It could be seen that this structure shows insignificant negative ARF effects in the range of 1.5 MHz–2.5 MHz.

Further, the PVC–water–PVC–water structure and its surrounding sound field in the process of frequency scanning are drawn in Fig. 11. Except that the suppression peak and the forward peak of backscattering are formed synchronously, the impedance parameters of organic materials and water have little difference compared with metal materials, the scattering effect is weakened, and the ARF is also reduced.

To sum up, it can be known that when the structure is reasonably designed to suppress the backscattering of the structure, the designed structure could be subjected to negative ARF, which provides a new idea for particle manipulation and makes the realization of “acoustic tweezers” possible.

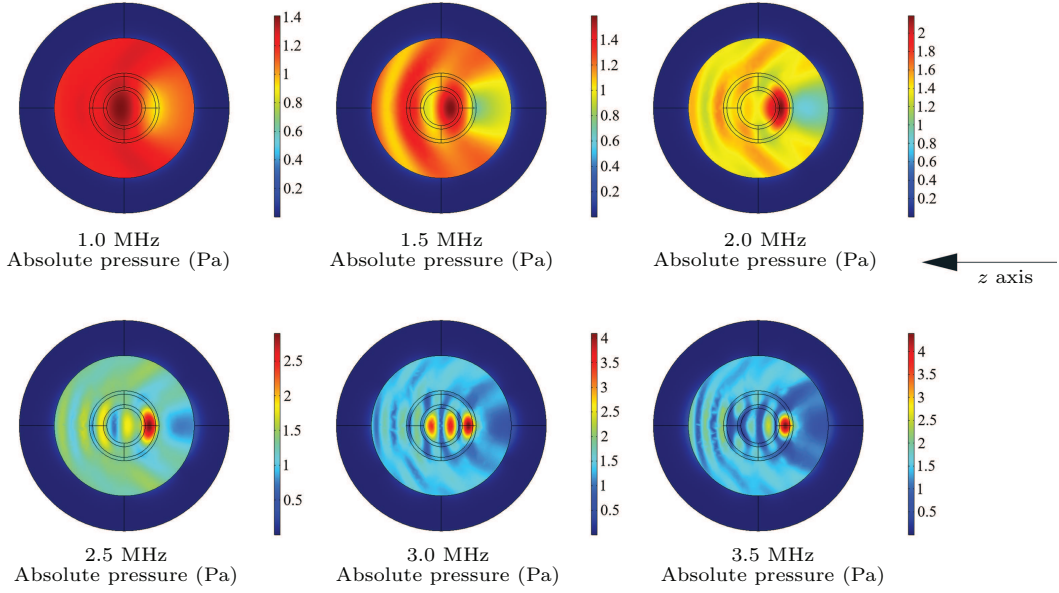


Fig. 11. Sound field distribution of PVC–water–PVC–water multiple-layered spherical structure with four-layer of 1 : 3 : 1 : 5 incident by unidirectional monochromatic wave. The frequency points are 1.0 MHz, 1.5 MHz, 2.0 MHz, 2.5 MHz, 3.0 MHz, and 3.5 MHz respectively.

4. Conclusion

This paper proposes a prediction of negative ARF based on a multiple-layered spherical structure. The ARF of the multiple-layered spherical structure is calculated and deduced, and the analytical solution is obtained. The physical mechanism of the negative acoustic radiation produced by multiple-layered spherical structure is described. This result is verified by finite element numerical simulations. This design concept is of great significance to the design of real “acoustic tweezers” based on negative ARF and lays a foundation for the design of devices producing negative ARF. This work proves that it is feasible to suppress backscattering to make the structure subject to negative ARF. In the process of designing a multi-layer structure to achieve negative ARF, we should try to choose a structural design that can significantly suppress backscattering, which is also the conjecture proposed by Marston before.^[38] In order to better realize this effect, we think that there should be a multiple-layered structure. Through numerical verification, the four-layered spheri-

cal structures with specific ratio could have a strong suppression effect on backscattering, thus exhibiting the anomalous characteristic of being subjected to negative acoustic radiation force. The different proportions of the thickness of the four-layered structure could form different resonant cavities, which can effectively adjust the scattering sound field of the structure, thereby achieving the suppression of backscattering. In the work, these specific scaling parameters are chosen as a result of extensive numerical calculations. In most of the parametric results, the inversion of the ARF does not appear. Further, based on the same mechanism, other structural designs are expected to be proposed. This work has broad application prospects in the fields of medicine, life science, underwater manipulation, and so on.

Appendix A

Matrix A_{1N} and matrix A_{2N} are expressed in Figs. A1 and A2.

$$\begin{bmatrix} b_1 & a_{1,2} & a_{1,3} & a_{1,4} & a_{1,5} & 0 & 0 & 0 & 0 & 0 & 0 & 0 & 0 & 0 & 0 & 0 & 0 & 0 & 0 & 0 & 0 \\ b_2 & a_{2,2} & a_{2,3} & a_{2,4} & a_{2,5} & 0 & 0 & 0 & 0 & 0 & 0 & 0 & 0 & 0 & 0 & 0 & 0 & 0 & 0 & 0 & 0 \\ 0 & a_{3,2} & a_{3,3} & a_{3,4} & a_{3,5} & 0 & 0 & 0 & 0 & 0 & 0 & 0 & 0 & 0 & 0 & 0 & 0 & 0 & 0 & 0 & 0 \\ 0 & a_{4,2} & a_{4,3} & a_{4,4} & a_{4,5} & a_{4,6} & a_{4,7} & a_{4,8} & a_{4,9} & 0 & 0 & 0 & 0 & 0 & 0 & 0 & 0 & 0 & 0 & 0 \\ 0 & a_{5,2} & a_{5,3} & a_{5,4} & a_{5,5} & a_{5,6} & a_{5,7} & a_{5,8} & a_{5,9} & 0 & 0 & 0 & 0 & 0 & 0 & 0 & 0 & 0 & 0 & 0 \\ 0 & a_{6,2} & a_{6,3} & a_{6,4} & a_{6,5} & a_{6,6} & a_{6,7} & a_{6,8} & a_{6,9} & 0 & 0 & 0 & 0 & 0 & 0 & 0 & 0 & 0 & 0 & 0 \\ 0 & a_{7,2} & a_{7,3} & a_{7,4} & a_{7,5} & a_{7,6} & a_{7,7} & a_{7,8} & a_{7,9} & 0 & 0 & 0 & 0 & 0 & 0 & 0 & 0 & 0 & 0 & 0 \\ 0 & 0 & 0 & 0 & 0 & a_{8,6} & a_{8,7} & a_{8,8} & a_{8,9} & a_{8,10} & a_{8,11} & a_{8,12} & a_{8,13} & 0 & 0 & 0 & 0 & 0 & 0 & 0 \\ 0 & 0 & 0 & 0 & 0 & a_{9,6} & a_{9,7} & a_{9,8} & a_{9,9} & a_{9,10} & a_{9,11} & a_{9,12} & a_{9,13} & 0 & 0 & 0 & 0 & 0 & 0 & 0 \\ 0 & 0 & 0 & 0 & 0 & a_{10,6} & a_{10,7} & a_{10,8} & a_{10,9} & a_{10,10} & a_{10,11} & a_{10,12} & a_{10,13} & 0 & 0 & 0 & 0 & 0 & 0 & 0 \\ 0 & 0 & 0 & 0 & 0 & a_{11,6} & a_{11,7} & a_{11,8} & a_{11,9} & a_{11,10} & a_{11,11} & a_{11,12} & a_{11,13} & 0 & 0 & 0 & 0 & 0 & 0 & 0 \\ 0 & 0 & 0 & 0 & 0 & \dots & 0 & 0 & 0 & 0 & 0 & 0 & 0 \\ 0 & 0 & 0 & 0 & 0 & 0 & 0 & 0 & a_{4m-8,4m-10} & a_{4m-8,4m-9} & a_{4m-8,4m-8} & a_{4m-8,4m-7} & a_{4m-8,4m-6} & a_{4m-8,4m-5} & a_{4m-8,4m-4} & a_{4m-8,4m-3} & 0 & 0 \\ 0 & 0 & 0 & 0 & 0 & 0 & 0 & 0 & a_{4m-7,4m-10} & a_{4m-7,4m-9} & a_{4m-7,4m-8} & a_{4m-7,4m-7} & a_{4m-7,4m-6} & a_{4m-7,4m-5} & a_{4m-7,4m-4} & a_{4m-7,4m-3} & 0 & 0 \\ 0 & 0 & 0 & 0 & 0 & 0 & 0 & 0 & a_{4m-6,4m-10} & a_{4m-6,4m-9} & a_{4m-6,4m-8} & a_{4m-6,4m-7} & a_{4m-6,4m-6} & a_{4m-6,4m-5} & a_{4m-6,4m-4} & a_{4m-6,4m-3} & 0 & 0 \\ 0 & 0 & 0 & 0 & 0 & 0 & 0 & 0 & a_{4m-5,4m-10} & a_{4m-5,4m-9} & a_{4m-5,4m-8} & a_{4m-5,4m-7} & a_{4m-5,4m-6} & a_{4m-5,4m-5} & a_{4m-5,4m-4} & a_{4m-5,4m-3} & 0 & 0 \\ 0 & 0 & 0 & 0 & 0 & 0 & 0 & 0 & 0 & 0 & 0 & 0 & a_{4m-4,4m-6} & a_{4m-4,4m-5} & a_{4m-4,4m-4} & a_{4m-4,4m-3} & a_{4m-4,4m-2} & a_{4m-4,4m-1} & 0 \\ 0 & 0 & 0 & 0 & 0 & 0 & 0 & 0 & 0 & 0 & 0 & 0 & a_{4m-3,4m-6} & a_{4m-3,4m-5} & a_{4m-3,4m-4} & a_{4m-3,4m-3} & a_{4m-3,4m-2} & a_{4m-3,4m-1} & 0 \\ 0 & 0 & 0 & 0 & 0 & 0 & 0 & 0 & 0 & 0 & 0 & 0 & a_{4m-2,4m-6} & a_{4m-2,4m-5} & a_{4m-2,4m-4} & a_{4m-2,4m-3} & a_{4m-2,4m-2} & a_{4m-2,4m-1} & 0 \\ 0 & 0 & 0 & 0 & 0 & 0 & 0 & 0 & 0 & 0 & 0 & 0 & a_{4m-1,4m-6} & a_{4m-1,4m-5} & a_{4m-1,4m-4} & a_{4m-1,4m-3} & a_{4m-1,4m-2} & a_{4m-1,4m-1} & 0 \end{bmatrix}$$

Fig. A1. Matrix A_{1N} .

$a_{1,1}$	$a_{1,2}$	$a_{1,3}$	$a_{1,4}$	$a_{1,5}$	0	0	0	0	0	0	0	0	0	0	0	0	0	0	0
$a_{2,1}$	$a_{2,2}$	$a_{2,3}$	$a_{2,4}$	$a_{2,5}$	0	0	0	0	0	0	0	0	0	0	0	0	0	0	0
0	$a_{3,2}$	$a_{3,3}$	$a_{3,4}$	$a_{3,5}$	0	0	0	0	0	0	0	0	0	0	0	0	0	0	0
0	$a_{4,2}$	$a_{4,3}$	$a_{4,4}$	$a_{4,5}$	$a_{4,6}$	$a_{4,7}$	$a_{4,8}$	$a_{4,9}$	0	0	0	0	0	0	0	0	0	0	0
0	$a_{5,2}$	$a_{5,3}$	$a_{5,4}$	$a_{5,5}$	$a_{5,6}$	$a_{5,7}$	$a_{5,8}$	$a_{5,9}$	0	0	0	0	0	0	0	0	0	0	0
0	$a_{6,2}$	$a_{6,3}$	$a_{6,4}$	$a_{6,5}$	$a_{6,6}$	$a_{6,7}$	$a_{6,8}$	$a_{6,9}$	0	0	0	0	0	0	0	0	0	0	0
0	$a_{7,2}$	$a_{7,3}$	$a_{7,4}$	$a_{7,5}$	$a_{7,6}$	$a_{7,7}$	$a_{7,8}$	$a_{7,9}$	0	0	0	0	0	0	0	0	0	0	0
0	0	0	0	0	$a_{8,6}$	$a_{8,7}$	$a_{8,8}$	$a_{8,9}$	$a_{8,10}$	$a_{8,11}$	$a_{8,12}$	$a_{8,13}$	0	0	0	0	0	0	0
0	0	0	0	0	$a_{9,6}$	$a_{9,7}$	$a_{9,8}$	$a_{9,9}$	$a_{9,10}$	$a_{9,11}$	$a_{9,12}$	$a_{9,13}$	0	0	0	0	0	0	0
0	0	0	0	0	$a_{10,6}$	$a_{10,7}$	$a_{10,8}$	$a_{10,9}$	$a_{10,10}$	$a_{10,11}$	$a_{10,12}$	$a_{10,13}$	0	0	0	0	0	0	0
0	0	0	0	0	$a_{11,6}$	$a_{11,7}$	$a_{11,8}$	$a_{11,9}$	$a_{11,10}$	$a_{11,11}$	$a_{11,12}$	$a_{11,13}$	0	0	0	0	0	0	0
0	0	0	0	0	0	0	0	0	0	0	0
0	0	0	0	0	0	0	0	0	$a_{4m-8,4m-10}$	$a_{4m-8,4m-9}$	$a_{4m-8,4m-8}$	$a_{4m-8,4m-7}$	$a_{4m-8,4m-6}$	$a_{4m-8,4m-5}$	$a_{4m-8,4m-4}$	$a_{4m-8,4m-3}$	0	0	
0	0	0	0	0	0	0	0	0	$a_{4m-7,4m-10}$	$a_{4m-7,4m-9}$	$a_{4m-7,4m-8}$	$a_{4m-7,4m-7}$	$a_{4m-7,4m-6}$	$a_{4m-7,4m-5}$	$a_{4m-7,4m-4}$	$a_{4m-7,4m-3}$	0	0	
0	0	0	0	0	0	0	0	0	$a_{4m-6,4m-10}$	$a_{4m-6,4m-9}$	$a_{4m-6,4m-8}$	$a_{4m-6,4m-7}$	$a_{4m-6,4m-6}$	$a_{4m-6,4m-5}$	$a_{4m-6,4m-4}$	$a_{4m-6,4m-3}$	0	0	
0	0	0	0	0	0	0	0	0	$a_{4m-5,4m-10}$	$a_{4m-5,4m-9}$	$a_{4m-5,4m-8}$	$a_{4m-5,4m-7}$	$a_{4m-5,4m-6}$	$a_{4m-5,4m-5}$	$a_{4m-5,4m-4}$	$a_{4m-5,4m-3}$	0	0	
0	0	0	0	0	0	0	0	0	0	0	0	0	$a_{4m-4,4m-6}$	$a_{4m-4,4m-5}$	$a_{4m-4,4m-4}$	$a_{4m-4,4m-3}$	$a_{4m-4,4m-2}$	$a_{4m-4,4m-1}$	
0	0	0	0	0	0	0	0	0	0	0	0	0	$a_{4m-3,4m-6}$	$a_{4m-3,4m-5}$	$a_{4m-3,4m-4}$	$a_{4m-3,4m-3}$	$a_{4m-3,4m-2}$	$a_{4m-3,4m-1}$	
0	0	0	0	0	0	0	0	0	0	0	0	0	$a_{4m-2,4m-6}$	$a_{4m-2,4m-5}$	$a_{4m-2,4m-4}$	$a_{4m-2,4m-3}$	$a_{4m-2,4m-2}$	$a_{4m-2,4m-1}$	
0	0	0	0	0	0	0	0	0	0	0	0	0	$a_{4m-1,4m-6}$	$a_{4m-1,4m-5}$	$a_{4m-1,4m-4}$	$a_{4m-1,4m-3}$	$a_{4m-1,4m-2}$	$a_{4m-1,4m-1}$	

Fig. A2. Matrix A_{2N} .

Here, for the boundary from the external medium to the first layer:

$$\begin{aligned}
b_1 &= x_{1,1,1} \mathbf{j}_n'(x_{1,1,1}), \\
b_2 &= -\frac{\rho_1}{\rho_2} x_{1,2,2}^2 \mathbf{j}_n(x_{1,1,1}), \\
a_{11} &= -x_{1,1,1} \mathbf{n}_n'(x_{1,1,1}), \\
a_{12} &= x_{1,2,1} \mathbf{j}_n'(x_{1,2,1}), \\
a_{13} &= x_{1,2,1} \mathbf{n}_n'(x_{1,2,1}), \\
a_{14} &= -n(n+1) \mathbf{j}_n(x_{1,2,2}), \\
a_{15} &= -n(n+1) \mathbf{n}_n(x_{1,2,2}), \\
a_{21} &= \frac{\rho_1}{\rho_2} x_{1,2,2}^2 \mathbf{h}_n^{(1)}(x_{1,1,1}), \\
a_{22} &= 2x_{1,2,1}^2 \mathbf{j}_n''(x_{1,2,1}) - (x_{1,2,2}^2 - 2x_{1,2,1}^2) \mathbf{j}_n(x_{1,2,1}), \\
a_{23} &= 2x_{1,2,1}^2 \mathbf{n}_n''(x_{1,2,1}) - (x_{1,2,2}^2 - 2x_{1,2,1}^2) \mathbf{n}_n(x_{1,2,1}), \\
a_{24} &= 2n(n+1) (\mathbf{j}_n(x_{1,2,2}) - x_{1,2,2} \mathbf{j}_n'(x_{1,2,2})), \\
a_{25} &= 2n(n+1) (\mathbf{n}_n(x_{1,2,2}) - x_{1,2,2} \mathbf{n}_n'(x_{1,2,2})), \\
a_{32} &= 2(x_{1,2,1} \mathbf{j}_n'(x_{1,2,1}) - \mathbf{j}_n(x_{1,2,1})), \\
a_{33} &= 2(x_{1,2,1} \mathbf{n}_n'(x_{1,2,1}) - \mathbf{n}_n(x_{1,2,1})), \\
a_{34} &= (2-n^2-n) \mathbf{j}_n(x_{1,2,2}) - x_{1,2,2}^2 \mathbf{j}_n''(x_{1,2,2}), \\
a_{35} &= (2-n^2-n) \mathbf{n}_n(x_{1,2,2}) - x_{1,2,2}^2 \mathbf{n}_n''(x_{1,2,2}).
\end{aligned}$$

For the boundary from the first layer to the second layer:

$$\begin{aligned}
a_{42} &= y_{21}j'_n(y_{21}), \\
a_{43} &= y_{21}n'_n(y_{21}), \\
a_{44} &= -n(n+1)j_n(y_{22}), \\
a_{45} &= -n(n+1)n_n(y_{22}), \\
a_{46} &= -y_{31}j'_n(y_{31}), \\
a_{47} &= -y_{31}n'_n(y_{31}), \\
a_{48} &= n(n+1)j_n(y_{32}), \\
a_{49} &= n(n+1)n_n(y_{32}), \\
a_{52} &= j_n(y_{21}), \\
a_{53} &= n_n(y_{21}), \\
a_{54} &= -y_{22}j'_n(y_{22}) - j_n(y_{22})
\end{aligned}$$

$$\begin{aligned}
a_{55} &= -y_{22}\mathbf{n}'_n(y_{22}) - \mathbf{n}_n(y_{22}), \\
a_{56} &= -\mathbf{j}_n(y_{31}), \\
a_{57} &= \mathbf{n}_n(y_{31}), \\
a_{58} &= y_{32}\mathbf{j}'_n(y_{32}) + \mathbf{j}_n(y_{32}), \\
a_{59} &= y_{32}\mathbf{n}'_n(y_{32}) + \mathbf{n}_n(y_{32}), \\
a_{62} &= 2\mu_2 y_{21}^2 \mathbf{j}''_n(y_{21}) - \lambda_2 y_{21}^2 \mathbf{j}_n(y_{21}), \\
a_{63} &= 2\mu_2 y_{21}^2 \mathbf{n}''_n(y_{21}) - \lambda_2 y_{21}^2 \mathbf{n}_n(y_{21}), \\
a_{64} &= 2\mu_2 n(n+1)(\mathbf{j}_n(y_{22}) - y_{22}\mathbf{j}'_n(y_{22})), \\
a_{65} &= 2\mu_2 n(n+1)(\mathbf{n}_n(y_{22}) - y_{22}\mathbf{n}'_n(y_{22})), \\
a_{66} &= -2\mu_3 y_{31}^2 \mathbf{j}''_n(y_{31}) + \lambda_3 y_{31}^2 \mathbf{j}_n(y_{31}), \\
a_{67} &= -2\mu_3 y_{31}^2 \mathbf{n}''_n(y_{31}) + \lambda_3 y_{31}^2 \mathbf{n}_n(y_{31}), \\
a_{68} &= 2\mu_3 n(n+1)(y_{32}\mathbf{j}'_n(y_{32}) - \mathbf{j}_n(y_{32})), \\
a_{69} &= 2\mu_3 n(n+1)(y_{32}\mathbf{j}'_n(y_{32}) - \mathbf{j}_n(y_{32})), \\
a_{72} &= 2\mu_2(y_{21}\mathbf{j}'_n(y_{21}) - \mathbf{j}_n(y_{21})), \\
a_{73} &= 2\mu_2(y_{21}\mathbf{n}'_n(y_{21}) - \mathbf{n}_n(y_{21})), \\
a_{74} &= (2-n^2-n)\mu_2\mathbf{j}_n(y_{22}) - \mu_2 y_{22}^2 \mathbf{j}''_n(y_{22}), \\
a_{75} &= (2-n^2-n)\mu_2\mathbf{n}_n(y_{22}) - \mu_2 y_{22}^2 \mathbf{n}''_n(y_{22}), \\
a_{76} &= 2\mu_3(\mathbf{j}_n(y_{31}) - y_{31}\mathbf{j}'_n(y_{31})), \\
a_{77} &= 2\mu_3(\mathbf{n}_n(y_{31}) - y_{31}\mathbf{n}'_n(y_{31})), \\
a_{78} &= (n^2+n-2)\mu_3\mathbf{j}_n(y_{32}) + \mu_3 y_{32}^2 \mathbf{j}''_n(y_{32}), \\
a_{79} &= (n^2+n-2)\mu_3\mathbf{n}_n(y_{32}) + \mu_3 y_{32}^2 \mathbf{n}''_n(y_{32}). \tag{A1}
\end{aligned}$$

For the boundary from the q -th to the $q+1$ -th layer which is not the innermost layer

$$\begin{aligned}
 a_{4q,4q-2} &= x_{q,q+1,1}\mathbf{j}'_n(x_{q,q+1,1}), \\
 a_{4q,4q-1} &= x_{q,q+1,1}\mathbf{n}'_n(x_{q,q+1,1}), \\
 a_{4q,4q} &= -n(n+1)\mathbf{j}_n(x_{q,q+1,2}), \\
 a_{4q,4q+1} &= -n(n+1)\mathbf{n}_n(x_{q,q+1,2}), \\
 a_{4q,4q+2} &= -x_{q,q+2,1}\mathbf{j}'_n(x_{q,q+2,1}), \\
 a_{4q,4q+3} &= -x_{q,q+2,1}\mathbf{n}'_n(x_{q,q+2,1}), \\
 a_{4q,4q+4} &= n(n+1)\mathbf{j}_n(x_{q,q+2,2}), \\
 a_{4q,4q+5} &= n(n+1)\mathbf{n}_n(x_{q,q+2,2}),
 \end{aligned}$$

$$\begin{aligned}
 a_{4q+1,4q-2} &= j_n(x_{q,q+1,1}), & a_{4q,4q+1} &= -n(n+1)n_n(x_{q,q+1,2}), \\
 a_{4q+1,4q-1} &= n_n(x_{q,q+1,1}), & a_{4q,4q+2} &= -x_{q,q+2,1}j'_n(x_{q,q+2,1}) - j_n(x_{q,q+2,1}), \\
 a_{4q+1,4q} &= -x_{q,q+1,2}j'_n(x_{q,q+1,2}) - j_n(x_{q,q+1,2}), & a_{4q,4q+3} &= n(n+1)j_n(x_{q,q+2,2}), \\
 a_{4q+1,4q+1} &= -x_{q,q+1,2}n'_n(x_{q,q+1,2}) - n_n(x_{q,q+1,2}), & a_{4q+1,4q-2} &= j_n(x_{q,q+1,1}), \\
 a_{4q+1,4q+2} &= -j_n(x_{q,q+2,1}), & a_{4q+1,4q-1} &= n_n(x_{q,q+1,1}), \\
 a_{4q+1,4q+3} &= n_n(x_{q,q+2,1}), & a_{4q+1,4q} &= -x_{q,q+1,2}j'_n(x_{q,q+1,2}) - j_n(x_{q,q+1,2}), \\
 a_{4q+1,4q+4} &= x_{q,q+2,2}j'_n(x_{q,q+2,2}) + j_n(x_{q,q+2,2}), & a_{4q+1,4q+1} &= -x_{q,q+1,2}n'_n(x_{q,q+1,2}) - n_n(x_{q,q+1,2}), \\
 a_{4q+1,4q+5} &= x_{q,q+2,2}n'_n(x_{q,q+2,2}) + n_n(x_{q,q+2,2}), & a_{4q+1,4q+2} &= -j_n(x_{q,q+2,1}), \\
 a_{4q+2,4q-2} &= 2\mu_{q+1}x_{q,q+1,1}^2j''_n(x_{q,q+1,1}) & a_{4q+1,4q+3} &= x_{q,q+2,2}j'_n(x_{q,q+2,2}) + j_n(x_{q,q+2,2}), \\
 &\quad - \lambda_2 x_{q,q+1,1}^2 j_n(x_{q,q+1,1}), & a_{4q+2,4q-2} &= 2\mu_{q+1}x_{q,q+1,1}^2j''_n(x_{q,q+1,1}) \\
 a_{4q+2,4q-1} &= 2\mu_{q+1}x_{q,q+1,1}^2n''_n(x_{q,q+1,1}) &&\quad - \lambda_2 x_{q,q+1,1}^2 j_n(x_{q,q+1,1}), \\
 &\quad - \lambda_2 x_{q,q+1,1}^2 n_n(x_{q,q+1,1}), & a_{4q+2,4q-1} &= 2\mu_{q+1}x_{q,q+1,1}^2n''_n(x_{q,q+1,1}) \\
 &\quad - \lambda_2 x_{q,q+1,1}^2 n_n(x_{q,q+1,1}), & a_{4q+2,4q} &= 2\mu_{q+1}n(n+1)(j_n(x_{q,q+1,2}) \\
 a_{4q+2,4q} &= 2\mu_{q+1}n(n+1)(j_n(x_{q,q+1,2}) &&\quad - x_{q,q+1,2}j'_n(x_{q,q+1,2})), \\
 &\quad - x_{q,q+1,2}j'_n(x_{q,q+1,2})), & a_{4q+2,4q+1} &= 2\mu_{q+1}n(n+1)(n_n(x_{q,q+1,2}) \\
 a_{4q+2,4q+1} &= 2\mu_{q+1}n(n+1)(n_n(x_{q,q+1,2}) &&\quad - x_{q,q+1,2}n'_n(x_{q,q+1,2})), \\
 &\quad - x_{q,q+1,2}n'_n(x_{q,q+1,2})), & a_{4q+2,4q+2} &= -2\mu_{q+2}x_{q,q+2,1}^2j''_n(x_{q,q+2,1}) \\
 a_{4q+2,4q+2} &= -2\mu_{q+2}x_{q,q+2,1}^2j''_n(x_{q,q+2,1}) &&\quad + \lambda_3 x_{q,q+2,1}^2 j_n(x_{q,q+2,1}), \\
 &\quad + \lambda_3 x_{q,q+2,1}^2 j_n(x_{q,q+2,1}), & a_{4q+2,4q+3} &= 2\mu_{q+2}n(n+1)(x_{q,q+2,2}j'_n(x_{q,q+2,2}) \\
 a_{4q+2,4q+3} &= -2\mu_{q+2}x_{q,q+2,1}^2n''_n(x_{q,q+2,1}) &&\quad - j_n(x_{q,q+2,2})), \\
 &\quad + \lambda_3 x_{q,q+2,1}^2 n_n(x_{q,q+2,1}), & a_{4q+3,4q-2} &= 2\mu_q(x_{q,q+1,1}j'_n(x_{q,q+1,1}) - j_n(x_{q,q+1,1})), \\
 a_{4q+2,4q+4} &= 2\mu_{q+2}n(n+1)(x_{q,q+2,2}j'_n(x_{q,q+2,2}) & a_{4q+3,4q-1} &= 2\mu_q(x_{q,q+1,1}n'_n(x_{q,q+1,1}) - n_n(x_{q,q+1,1})), \\
 &\quad - j_n(x_{q,q+2,2})), & a_{4q+3,4q} &= (2-n^2-n)\mu_q j_n(x_{q,q+1,2}) \\
 a_{4q+2,4q+5} &= 2\mu_{q+2}n(n+1)(x_{q,q+2,2}n'_n(x_{q,q+2,2}) &&\quad - \mu_q x_{q,q+1,2}^2 j''_n(x_{q,q+1,2})), \\
 &\quad - n_n(x_{q,q+2,2})), & a_{4q+3,4q+1} &= (2-n^2-n)\mu_q j_n(x_{q,q+1,2}) \\
 a_{4q+3,4q-2} &= 2\mu_q(x_{q,q+1,1}j'_n(x_{q,q+1,1}) - j_n(x_{q,q+1,1})), &&\quad - \mu_q x_{q,q+1,2}^2 j''_n(x_{q,q+1,2})), \\
 a_{4q+3,4q-1} &= 2\mu_q(x_{q,q+1,1}n'_n(x_{q,q+1,1}) - n_n(x_{q,q+1,1})), & a_{4q+3,4q+2} &= (2-n^2-n)\mu_q j_n(x_{q,q+1,2}) \\
 a_{4q+3,4q} &= (2-n^2-n)\mu_q j_n(x_{q,q+1,2}) &&\quad - \mu_q x_{q,q+1,2}^2 j''_n(x_{q,q+1,2})), \\
 &\quad - \mu_q x_{q,q+1,2}^2 j''_n(x_{q,q+1,2}), & a_{4q+3,4q+3} &= 2\mu_{q+1}(j_n(x_{q,q+2,1}) - x_{q,q+2,1}j'_n(x_{q,q+2,1})), \\
 a_{4q+3,4q+1} &= (2-n^2-n)\mu_q n_n(x_{q,q+1,2}) & a_{4q+3,4q+4} &= (n^2+n-2)\mu_{q+1}j_n(x_{q,q+2,2}) \\
 &\quad - \mu_q x_{q,q+1,2}^2 n''_n(x_{q,q+1,2}), &&\quad + \mu_{q+1}x_{q,q+2,2}^2 j''_n(x_{q,q+2,2}). \tag{A2}
 \end{aligned}$$

For the boundary from the q -th to the $q+1$ -th layer which is the innermost layer

$$\begin{aligned}
 a_{4q,4q-2} &= x_{q,q+1,1}j'_n(x_{q,q+1,1}), \\
 a_{4q,4q-1} &= x_{q,q+1,1}n'_n(x_{q,q+1,1}), \\
 a_{4q,4q} &= -n(n+1)j_n(x_{q,q+1,2}),
 \end{aligned}$$

$$\begin{aligned}
 x_{q,q,1} &= \frac{r_q}{r_1}x_{1,q,1}, \\
 x_{q,q,2} &= \frac{r_q}{r_1}x_{1,q,2}, \\
 x_{q,q+1,1} &= \frac{r_q}{r_1}x_{1,q+1,1}, \\
 x_{q,q+1,2} &= \frac{r_q}{r_1}x_{1,q+1,2}, \\
 x_{1,q,1} &= \frac{x_1 c_1 (1+i\gamma_{q,1})}{c_{q,1}}, \\
 x_{1,q,2} &= \frac{x_1 c_1 (1+i\gamma_{q,2})}{c_{q,2}}, \\
 x_{1,q+1,1} &= \frac{x_1 c_1 (1+i\gamma_{q+1,1})}{c_{q+1,1}},
 \end{aligned}$$

$$x_{1,q+1,2} = \frac{x_1 c_1 (1 + i \gamma_{q+1,2})}{c_{q+1,2}},$$

where, $c_{q+1,1}$ is the longitudinal wave velocity of the q -th layer structure, $c_{q+1,2}$ is the shear wave velocity of the q -th layer structure. $\gamma_{q+1,1}$ is the longitudinal wave absorption coefficient of the q -th layer medium, $\gamma_{q+1,2}$ is the longitudinal wave absorption coefficient of the q -th layer medium. μ_{q+1} and λ_{q+1} are the density coefficients of the q -th layer.

Acknowledgements

Project supported by the National Key Research and Development Program of China (Grant No. 2020YFA0211400), the State Key Program of the National Natural Science Foundation of China (Grant No. 11834008), the National Natural Science Foundation of China (Grant Nos. 12174192 and 12204119), the Fund from the State Key Laboratory of Acoustics, Chinese Academy of Sciences (Grant No. SKLA202210), the Fund from the Key Laboratory of Underwater Acoustic Environment, Chinese Academy of Sciences (Grant No. SSHJ-KFKT-1701), and the Science and Technology Foundation of Guizhou Province, China (Grant No. ZK[2023]249).

References

- [1] Ashkin A 1992 *Biophys. J.* **61** 569
- [2] Wu J R 1991 *J. Acoust. Soc. Am.* **89** 2140
- [3] Baresch D, Thomas J L and Marchiano R 2013 *J. Appl. Phys.* **113** 184901
- [4] Baresch D, Thomas J L and Marchiano R 2016 *Phys. Rev. Lett.* **116** 024301
- [5] Fan X D and Zhang L 2021 *J. Acoust. Soc. Am.* **150** 102
- [6] Gong Z X, Marston P L, Li W and Chai Y B 2017 *J. Acoust. Soc. Am.* **141** El574
- [7] Marston P L 2006 *J. Acoust. Soc. Am.* **120** 3518
- [8] Marston P L 2009 *J. Acoust. Soc. Am.* **125** 3539
- [9] Marston P L 2017 *Phys. Fluids* **29** 029101
- [10] Mitri F G 2016 *Phys. Fluids* **28** 077104
- [11] Sapozhnikov O A and Bailey M R 2013 *J. Acoust. Soc. Am.* **133** 661
- [12] Wang H B, Gao S, Qiao Y P, Liu J H and Liu X Z 2019 *Phys. Fluids* **31** 047103
- [13] Wu R R, Cheng K X, Liu X Z, Liu J H, Gong X F and Li Y F 2016 *Wave Motion* **62** 63
- [14] Wu R R, Cheng K X, Liu X Z, Liu J H, Mao Y W and Gong X F 2014 *J. Acoust. Soc. Am.* **116** 144903
- [15] Zhang L K and Marston P L 2011 *Phys. Rev. E* **84** 035601
- [16] Zhang L K and Marston P L 2012 *J. Acoust. Soc. Am.* **131** El329
- [17] Qiao Y P, Gong M Y, Wang H B, Lan J, Liu T, Liu J H, Mao Y W, He A J and Liu X Z 2021 *Phys. Fluids* **33** 047107
- [18] Gong M Y, Xu X, Qiao Y P, Fei Z H, Li Y Y, Liu J H, He A J and Liu X Z 2023 *Results in Physics* **46** 106264
- [19] Gong M Y, Xu X, Fei Z H, Li Y Y, Liu T, Gao S L, Liu J H, He A J and Liu X Z 2023 *J. Acoust. Soc. Am.* **153** 812
- [20] Gong M Y, Qiao Y P, Lan J and Liu X Z 2020 *Phys. Fluids* **32** 117104
- [21] Gong M Y, Shi M J, Li Y Y, Xu X, Fei Z H, Qiao Y P, Liu J H, He A J and Liu X Z 2023 *Phys. Fluids* **35** 057108
- [22] Gong Z X and Baudoin M 2021 *J. Acoust. Soc. Am.* **149** 3469
- [23] Wang Q, Riaud A, Zhou J, Gong Z X and Baudoin M 2021 *Phys. Rev. Appl.* **15** 044034
- [24] Baresch D, Thomas J L and Marchiano R 2013 *J. Acoust. Soc. Am.* **133** 25
- [25] Hasegawa T, Hino Y, Annou A, Noda H, Kato M and Inoue N 1993 *J. Acoust. Soc. Am.* **93** 154
- [26] Marston P L 2019 *J. Acoust. Soc. Am.* **146** EL145
- [27] Zhang L and Marston P L 2016 *J. Acoust. Soc. Am.* **140** EL178
- [28] Doinikov A A 1994 *Proceedings of the Royal Society-Mathematical and Physical Sciences* **447** 447
- [29] Wiklund M, Green R and Ohlin M 2012 *Lab on a Chip* **12** 2438
- [30] Johnson K A, Vormohr H R, Doinikov A A, Bouakaz A, Shields C W, Lopez G P and Dayton P A 2016 *Phys. Rev. E* **93** 053109
- [31] Gong K M, Zhou X, Ouyang H J and Mo J L 2021 *J. Phys. D: Appl. Phys.* **54** 305302
- [32] Leshno A, Kenigsberg A, Peleg-Levy H, Piperno S, Skaat A and Shpaisman H 2022 *Micromachines* **13** 1362
- [33] Pan H M, Mei D Q, Xu C Y, Li X and Wang Y C 2023 *Journal of Colloid and Interface Science* **643** 115
- [34] Hoque S Z, Nath A and Sen A K 2021 *J. Acoust. Soc. Am.* **150** 307
- [35] Marston P L, Daniel T D, Fortuner A R, Kirsteins I P and Abawi A T 2021 *J. Acoust. Soc. Am.* **149** 3042
- [36] Leao-Neto J P, Hoyos M, Aider J L and Silva G T 2021 *J. Acoust. Soc. Am.* **149** 285
- [37] Gong M Y, Qiao Y P, Fei Z H, Li Y Y, Liu J H, Mao Y W, He A J and Liu X Z 2021 *AIP Adv.* **11** 065029
- [38] Marston P L 2007 *J. Acoust. Soc. Am.* **122** 3162
- [39] Gong Z X, Marston P L and Li W 2019 *Phys. Rev. E* **99** 063004
- [40] Leibacher I, Dietze W, Hahn P, Wang J T, Schmitt S and Dual J 2014 *Microfluidics and Nanofluidics* **16** 513
- [41] Rajabi M and Mojahed A 2018 *Ultrasonics* **83** 146

Chinese Physics B

Volume 33 Number 1 January 2024

Contents

TOPICAL REVIEW — Valleytronics

- 017203 Valley filtering and valley-polarized collective modes in bulk graphene monolayers
Jian-Long Zheng and Feng Zhai
- 017306 Recent progress on valley polarization and valley-polarized topological states in two-dimensional materials
Fei Wang, Yaling Zhang, Wenjia Yang, Huisheng Zhang and Xiaohong Xu
- 017505 Progress on two-dimensional ferrovalley materials
Ping Li, Bang Liu, Shuai Chen, Wei-Xi Zhang and Zhi-Xin Guo
- 017801 Valley transport in Kekulé structures of graphene
Juan-Juan Wang and Jun Wang

SPECIAL TOPIC — Valleytronics

- 016303 Optical spectrum of ferrovalley materials: A case study of Janus H-VSSe
Chao-Bo Luo, Wen-Chao Liu and Xiang-Yang Peng
- 017205 Valley-dependent transport in a mesoscopic twisted bilayer graphene device
Wen-Xuan Shi, Han-Lin Liu and Jun Wang
- 018502 Valleytronic topological filters in silicene-like inner-edge systems
Hang Xie, Xiao-Long Lü and Jia-En Yang

TOPICAL REVIEW — States and new effects in nonequilibrium

- 010301 Progress and realization platforms of dynamic topological photonics
Qiu-Chen Yan, Rui Ma, Xiao-Yong Hu and Qi-Huang Gong
- 010701 Capturing the non-equilibrium state in light-matter-free-electron interactions through ultrafast transmission electron microscopy
Wentao Wang, Shuaishuai Sun, Jun Li, Dingguo Zheng, Siyuan Huang, Huanfang Tian, Huaixin Yang and Jianqi Li
- 013201 Attosecond ionization time delays in strong-field physics
Yongzhe Ma, Hongcheng Ni and Jian Wu
- 017204 Photophysics of metal-organic frameworks: A brief overview
Qingshuo Liu, Junhong Yu and Jianbo Hu

(Continued on the Bookbinding Inside Back Cover)

SPECIAL TOPIC — States and new effects in nonequilibrium

- 016101 **Universal basis underlying temperature, pressure and size induced dynamical evolution in metallic glass-forming liquids**
H P Zhang, B B Fan, J Q Wu and M Z Li
- 016102 **Anelasticity to plasticity transition in a model two-dimensional amorphous solid**
Baoshuang Shang
- 016103 **Ultrafast dynamics in photo-excited Mott insulator $\text{Sr}_3\text{Ir}_2\text{O}_7$ at high pressure**
Xia Yin, Jianbo Zhang, Wang Dong, Takeshi Nakagawa, Chunsheng Xia, Caoshun Zhang, Weicheng Guo, Jun Chang and Yang Ding
- 016301 ***Ab initio* nonadiabatic molecular dynamics study on spin-orbit coupling induced spin dynamics in ferromagnetic metals**
Wansong Zhu, Zhenfa Zheng, Qijing Zheng and Jin Zhao
- 017201 **Ultrafast carrier dynamics in GeSn thin film based on time-resolved terahertz spectroscopy**
Panpan Huang, Youlu Zhang, Kai Hu, Jingbo Qi, Dainan Zhang and Liang Cheng
- 017901 **Optical manipulation of the topological phase in ZrTe_5 revealed by time- and angle-resolved photoemission**
Chaozhi Huang, Chengyang Xu, Fengfeng Zhu, Shaofeng Duan, Jianzhe Liu, Lingxiao Gu, Shichong Wang, Haoran Liu, Dong Qian, Weidong Luo and Wentao Zhang
- 018702 **Core-level spectroscopy of the photodissociation process of BrCN molecule**
Kun Zhou and Han Wang

INSTRUMENTATION AND MEASUREMENT

- 010702 **A step to the decentralized real-time timekeeping network**
Fangmin Wang, Yufeng Chen, Jianhua Zhou, Yuting Lin, Jun Yang, Bo Wang and Lijun Wang
- 017301 **Design and simulation of an accelerometer based on NV center spin-strain coupling**
Lu-Min Ji, Li-Ye Zhao and Yu-Hai Wang

RAPID COMMUNICATION

- 010302 **Sharing quantum nonlocality in the noisy scenario**
Shu-Yuan Yang, Jin-Chuan Hou and Kan He
- 010303 **Observation of flat-band localized state in a one-dimensional diamond momentum lattice of ultracold atoms**
Chao Zeng, Yue-Ran Shi, Yi-Yi Mao, Fei-Fei Wu, Yan-Jun Xie, Tao Yuan, Han-Ning Dai and Yu-Ao Chen
- 017202 **Higher-order topological Anderson insulator on the Sierpiński lattice**
Huan Chen, Zheng-Rong Liu, Rui Chen and Bin Zhou

- 017404 Effects of carrier density and interactions on pairing symmetry in a t_{2g} model**
Yun-Xiao Li, Wen-Han Xi, Zhao-Yang Dong, Zi-Jian Yao, Shun-Li Yu and Jian-Xin Li
- 017802 Optical study of magnetic topological insulator $MnBi_4Te_7$**
Zhi-Yu Liao, Bing Shen, Xiang-Gang Qiu and Bing Xu
- 018801 Maskless fabrication of quasi-omnidirectional V-groove solar cells using an alkaline solution-based method**
Xingqian Chen, Yan Wang, Wei Chen, Yaoping Liu, Guoguang Xing, Bowen Feng, Haozhen Li, Zongheng Sun and Xiaolong Du

GENERAL

- 010201 Efficient method to calculate the eigenvalues of the Zakharov–Shabat system**
Shikun Cui and Zhen Wang
- 010202 A deep learning method based on prior knowledge with dual training for solving FPK equation**
Denghui Peng, Shenlong Wang and Yuanchen Huang
- 010203 Research and application of composite stochastic resonance in enhancement detection**
Rui Gao, Shangbin Jiao and Qiongjie Xue
- 010304 Threshold-independent method for single-shot readout of spin qubits in semiconductor quantum dots**
Rui-Zi Hu, Sheng-Kai Zhu, Xin Zhang, Yuan Zhou, Ming Ni, Rong-Long Ma, Gang Luo, Zhen-Zhen Kong, Gui-Lei Wang, Gang Cao, Hai-Ou Li and Guo-Ping Guo
- 010501 An underdamped and delayed tri-stable model-based stochastic resonance**
Yan-Fei Jin, Hao-Tian Wang and Ting-Ting Zhang
- 010502 Enhancing visual security: An image encryption scheme based on parallel compressive sensing and edge detection embedding**
Yiming Wang, Shufeng Huang, Huang Chen, Jian Yang and Shuting Cai
- 010503 Characteristic analysis of 5D symmetric Hamiltonian conservative hyperchaotic system with hidden multiple stability**
Li-Lian Huang, Yan-Hao Ma and Chuang Li
- 010703 Static-to-kinematic modeling and experimental validation of tendon-driven quasi continuum manipulators with nonconstant subsegment stiffness**
Xian-Jie Zheng, Meng Ding, Liao-Xue Liu, Lu Wang and Yu Guo

ATOMIC AND MOLECULAR PHYSICS

- 013101 *Ab initio* potential energy surface and anharmonic vibration spectrum of NF_3^+**
Yan-Nan Chen, Jian-Gang Xu, Jiang-Peng Fan, Shuang-Xiong Ma, Tian Guo and Yun-Guang Zhang

- 013102 High-order harmonic generation of ZnO crystals in chirped and static electric fields**
Ling-Yu Zhang, Yong-Lin He, Zhuo-Xuan Xie, Fang-Yan Gao, Qing-Yun Xu, Xin-Lei Ge, Xiang-Yi Luo and Jing Guo
- 013301 Collision off-axis position dependence of relativistic nonlinear Thomson inverse scattering of an excited electron in a tightly focused circular polarized laser pulse**
Yubo Wang, Qingyu Yang, Yifan Chang, Zongyi Lin and Youwei Tian
- 013302 Internal collision double ionization of molecules driven by co-rotating two-color circularly polarized laser pulses**
Xue-Feng Li, Yue Qiao, Dan Wu, Rui-Xian Yu, Ji-Gen Chen, Jun Wang, Fu-Ming Guo and Yu-Jun Yang
- 013303 Electron vortices generation of photoelectron of H_2^+ by counter-rotating circularly polarized attosecond pulses**
Haojing Yang, Xiaoyu Liu, Fengzheng Zhu, Liguang Jiao and Aihua Liu
- ELECTROMAGNETISM, OPTICS, ACOUSTICS, HEAT TRANSFER, CLASSICAL MECHANICS, AND FLUID DYNAMICS**
- 014101 Electric field and force characteristic of dust aerosol particles on the surface of high-voltage transmission line**
Yingge Liu, Xingcai Li, Juan Wang, Xin Ma and Wenhai Sun
- 014102 Intensity correlation properties of x-ray beams split with Laue diffraction**
Chang-Zhe Zhao, Shang-Yu Si, Hai-Peng Zhang, Lian Xue, Zhong-Liang Li and Ti-Qiao Xiao
- 014201 A 1-bit electronically reconfigurable beam steerable metasurface reflectarray with multiple polarization manipulations**
Yan Shi, Xi-Ya Xu, Shao-Ze Wang, Wen-Yue Wei and Quan-Wei Wu
- 014202 Young's double slit interference with vortex source**
Qilin Duan, Pengfei Zhao, Yuhang Yin and Huanyang Chen
- 014203 Phase sensitivity with a coherent beam and twin beams via intensity difference detection**
Jun Liu, Tao Shao, Chenlu Li, Minyang Zhang, Youyou Hu, Dongxu Chen and Dong Wei
- 014204 Bessel-Gaussian beam-based orbital angular momentum holography**
Jiaying Ji, Zhigang Zheng, Jialong Zhu, Le Wang, Xinguang Wang and Shengmei Zhao
- 014205 Finesse measurement for high-power optical enhancement cavity**
Xin-Yi Lu, Xing Liu, Qi-Li Tian, Huan Wang, Jia-Jun Wang and Li-Xin Yan
- 014206 Using harmonic beam combining to generate pulse-burst in nonlinear optical laser**
Yuan-Zhai Xu, Zhen-Ling Li, Ao-Nan Zhang, Ke Liu, Jing-Jing Zhang, Xiao-Jun Wang, Qin-Jun Peng and Zu-Yan Xu

014207 Giant and controllable Goos–Hänchen shift of a reflective beam off a hyperbolic meta-surface of polar crystals

Tian Xue, Yu-Bo Li, Hao-Yuan Song, Xiang-Guang Wang, Qiang Zhang, Shu-Fang Fu, Sheng Zhou and Xuan-Zhang Wang

014208 Quasi-anti-parity-time-symmetric single-resonator micro-optical gyroscope with Kerr nonlinearity

Jingtong Geng, Shuyi Xu, Ting Jin, Shulin Ding, Liu Yang, Ying Wang and Yonggang Zhang

014209 Performance analysis of single-focus phase singularity based on elliptical reflective annulus quadrangle-element coded spiral zone plates

Huaping Zang, Baozhen Wang, Chenglong Zheng, Lai Wei, Quanping Fan, Shaoyi Wang, Zuhua Yang, Weimin Zhou, Leifeng Cao and Haizhong Guo

014210 Effective transmittance of Fabry–Perot cavity under non-parallel beam incidence

Yin-Sheng Lv, Pin-Hua Xie, Jin Xu, You-Tao Li and Hua-Rong Zhang

014211 Terahertz quasi-perfect vortex beam with integer-order and fractional-order generated by spiral spherical harmonic axicon

Si-Yu Tu, De-Feng Liu, Jin-Song Liu, Zhen-Gang Yang and Ke-Jia Wang

014301 Effects of confining pressure and pore pressure on multipole borehole acoustic field in fluid-saturated porous media

Zhi-Qiang Zhao, Jin-Xia Liu, Jian-Yu Liu and Zhi-Wen Cui

014302 Scheme of negative acoustic radiation force based on a multiple-layered spherical structure

Menyang Gong, Xin Xu, Yupei Qiao, Jiehui Liu, Aijun He and Xiaozhou Liu

014303 Discrete multi-step phase hologram for high frequency acoustic modulation

Meng-Qing Zhou, Zhao-Xi Li, Yi Li, Ye-Cheng Wang, Juan Zhang, Dong-Dong Chen, Yi Quan, Yin-Tang Yang and Chun-Long Fei

PHYSICS OF GASES, PLASMAS, AND ELECTRIC DISCHARGES

015201 Electron characteristics and dynamics in sub-millimeter pulsed atmospheric dielectric barrier discharge

Junlin Fang, Yarong Zhang, Chenzi Lu, Lili Gu, Shaofeng Xu, Ying Guo and Jianjun Shi

015202 Numerical study of alpha particle loss with toroidal field ripple based on CFETR steady-state scenario

Niuqi Li, Yingfeng Xu, Fangchuan Zhong and Debing Zhang

015203 Growth mechanism and characteristics of electron drift instability in Hall thruster with different propellant types

Long Chen, Zi-Chen Kan, Wei-Fu Gao, Ping Duan, Jun-Yu Chen, Cong-Qi Tan and Zuo-Jun Cui

- 015204 Fluid-chemical modeling of the near-cathode sheath formation process in a high current broken in DC air circuit breaker**

Shi-Dong Peng, Jing Li, Wei Duan, Yun-Dong Cao, Shu-Xin Liu and Hao Huang

- 015205 Transition from a filamentary mode to a diffuse one with varying distance from needle to stream of an argon plasma jet**

Hui-Min Xu, Jing-Ge Gao, Peng-Ying Jia, Jun-Xia Ran, Jun-Yu Chen and Jin-Mao Li

- 015206 Suppression of stimulated Brillouin and Raman scatterings using an alternating frequency laser and transverse magnetic fields**

Rui-Jin Cheng, Xiao-Xun Li, Qing Wang, De-Ji Liu, Zhuo-Ming Huang, Shuai-Yu Lv, Yuan-Zhi Zhou, Shu-Tong Zhang, Xue-Ming Li, Zu-Jie Chen, Qiang Wang, Zhan-Jun Liu, Li-Hua Cao and Chun-Yang Zheng

CONDENSED MATTER: STRUCTURAL, MECHANICAL, AND THERMAL PROPERTIES

- 016104 Sensitivity investigation of 100-MeV proton irradiation to SiGe HBT single event effect**

Ya-Hui Feng, Hong-Xia Guo, Yi-Wei Liu, Xiao-Ping Ouyang, Jin-Xin Zhang, Wu-Ying Ma, Feng-Qi Zhang, Ru-Xue Bai, Xiao-Hua Ma and Yue Hao

- 016105 Effect of grain size on gas bubble evolution in nuclear fuel: Phase-field investigations**

Dan Sun, Qingfeng Yang, Jiajun Zhao, Shixin Gao, Yong Xin, Yi Zhou, Chunyu Yin, Ping Chen, Jijun Zhao and Yuanyuan Wang

- 016106 Simulation of space heavy-ion induced primary knock-on atoms in bipolar devices**

Bin Zhang, Hao Jiang, Xiao-Dong Xu, Tao Ying, Zhong-Li Liu, Wei-Qi Li, Jian-Qun Yang and Xing-Ji Li

- 016107 Hamiltonian system for the inhomogeneous plane elasticity of dodecagonal quasicrystal plates and its analytical solutions**

Zhiqiang Sun, Guolin Hou, Yanfen Qiao and Jincun Liu

- 016108 Linear magnetoresistance and structural distortion in layered $\text{SrCu}_{4-x}\text{P}_2$ single crystals**

Yong Nie, Zheng Chen, Wensen Wei, Huijie Li, Yong Zhang, Ming Mei, Yuanyuan Wang, Wenhai Song, Dongsheng Song, Zhaosheng Wang, Xiangde Zhu, Wei Ning and Mingliang Tian

- 016109 Geometries and electronic structures of Zr_nCu ($n = 2-12$) clusters: A joint machine-learning potential density functional theory investigation**

Yizhi Wang, Xiuhua Cui, Jing Liu, Qun Jing, Haiming Duan and Haibin Cao

- 016201 Temperature effect on nanotwinned Ni under nanoindentation using molecular dynamic simulation**

Xi He, Ziyi Xu and Yushan Ni

016202 Atomistic evaluation of tension–compression asymmetry in nanoscale body-centered-cubic AlCrFeCoNi high-entropy alloy

Runlong Xing and Xuepeng Liu

016302 Determining Hubbard U of VO₂ by the quasi-harmonic approximation

Longjuan Kong, Yuhang Lu, Xinying Zhuang, Zhiyong Zhou and Zhenpeng Hu

016801 Effects of Mg-doping temperature on the structural and electrical properties of nonpolar a -plane p-type GaN films

Kai Chen, Jianguo Zhao, Yu Ding, Wenxiao Hu, Bin Liu, Tao Tao, Zhe Zhuang, Yu Yan, Zili Xie, Jianhua Chang, Rong Zhang and Youliao Zheng

CONDENSED MATTER: ELECTRONIC STRUCTURE, ELECTRICAL, MAGNETIC, AND OPTICAL PROPERTIES

017101 Majorana noise model and its influence on the power spectrum

Shumeng Chen, Sifan Ding, Zhen-Tao Zhang and Dong E. Liu

017102 Quantitative determination of the critical points of Mott metal–insulator transition in strongly correlated systems

Yuekun Niu, Yu Ni, Jianli Wang, Leiming Chen, Ye Xing, Yun Song and Shiping Feng

017302 Physical mechanism of oxygen diffusion in the formation of Ga₂O₃ Ohmic contacts

Su-Yu Xu, Miao Yu, Dong-Yang Yuan, Bo Peng, Lei Yuan, Yu-Ming Zhang and Ren-Xu Jia

017303 Resistive switching behavior and mechanism of HfO_x films with large on/off ratio by structure design

Xianglin Huang, Ying Wang, Huixiang Huang, Li Duan and Tingting Guo

017304 Electrically controllable spin filtering in zigzag phosphorene nanoribbon based normal–antiferromagnet–normal junctions

Ruigang Li, Jun-Feng Liu and Jun Wang

017305 Electric modulation of the Fermi arc spin transport via three-terminal configuration in topological semimetal nanowires

Guang-Yu Zhu, Ji-Ai Ning, Jian-Kun Wang, Xin-Jie Liu, Jia-Jie Yang, Ben-Chuan Lin and Shuo Wang

017401 Distinct behavior of electronic structure under uniaxial strain in BaFe₂As₂

Jiajun Li, Giao Ngoc Phan, Xingyu Wang, Fazhi Yang, Quanxin Hu, Ke Jia, Jin Zhao, Wenyao Liu, Renjie Zhang, Youguo Shi, Shiliang Li, Tian Qian and Hong Ding

017402 Enhanced conductivity and weakened magnetism in Pb-doped Sr₂IrO₄

Zhi-Lai Yue, Wei-Li Zhen, Rui Niu, Ke-Ke Jiao, Wen-Ka Zhu, Li Pi and Chang-Jin Zhang

017403 Majorana tunneling in a one-dimensional wire with non-Hermitian double quantum dots

Peng-Bin Niu and Hong-Gang Luo

- 017501 Tunable dispersion relations manipulated by strain in skyrmion-based magnonic crystals**
Zhao-Nian Jin, Xuan-Lin He, Chao Yu, Henan Fang, Lin Chen and Zhi-Kuo Tao
- 017502 Magnetic and electronic properties of La-doped hexagonal 4H-SrMnO₃**
Jie Li, Yinan Chen, Nuo Gong, Xin Huang, Zhihong Yang and Yakui Weng
- 017503 Controllable high Curie temperature through 5d transition metal atom doping in CrI₃**
Xuebing Peng, Mingsu Si and Daqiang Gao
- 017504 Stacking-dependent exchange bias in two-dimensional ferromagnetic/antiferromagnetic bilayers**
Huiping Li, Shuaiwei Pan, Zhe Wang, Bin Xiang and Wenguang Zhu
- 017803 Shape and diffusion instabilities of two non-spherical gas bubbles under ultrasonic conditions**
Wurihan Bao and De-Xin Wang

INTERDISCIPLINARY PHYSICS AND RELATED AREAS OF SCIENCE AND TECHNOLOGY

- 018101 Epitaxial growth of ultrathin gallium films on Cd(0001)**
Zuo Li, Mingxia Shi, Gang Yao, Minlong Tao and Junzhong Wang
- 018501 High responsivity photodetectors based on graphene/WSe₂ heterostructure by photogating effect**
Shuping Li, Ting Lei, Zhongxing Yan, Yan Wang, Like Zhang, Huayao Tu, Wenhua Shi and Zhongming Zeng
- 018701 Quantitative analysis of the morphing wing mechanism of raptors: IMMU-based motion capture system and its application on gestures of a *Falco peregrinus***
Di Tang, Liwen Zhu, Wenxi Shi, Dawei Liu, Yin Yang, Guorong Yao, Senxiang Yan, Zhongyong Fan, Yiwei Lu and Siyu Wang
- 018901 Identifying influential spreaders in social networks: A two-stage quantum-behaved particle swarm optimization with Lévy flight**
Pengli Lu, Jimao Lan, Jianxin Tang, Li Zhang, Shihui Song and Hongyu Zhu
- 018902 Pedestrian flow through exit: Study focused on evacuation pattern**
Bo-Si Zhang, Zhi-Hong Yu, Bo-Lin Sun, Zi-Yu Guo and Mo Chen
- 018903 Essential proteins identification method based on four-order distances and subcellular localization information**
Pengli Lu, Yu Zhong and Peishi Yang
- 018904 Analysis of radiation diffusion of COVID-19 driven by social attributes**
Fuzhong Nian, Xiaochen Yang and Yayong Shi